Natural Environment Research Council

Institute of Geological Sciences

Mineral Reconnaissance Programme Report

A report prepared for the Department of Industry

D. Ostle
Programme Manager
Institute of Geological Sciences
Keyworth,
Nottingham NG12 5GG

No. 43

Disseminated copper-molybdenum mineralisation near Ballachulish, Highland Region

INSTITUTE OF GEOLOGICAL SCIENCES

Natural Environment Research Council

Mineral Reconnaissance Programme

Report No. 43

Disseminated copper-molybdenum mineralisation near Ballachulish, Highland Region

Geology and geochemistry
H. W. Haslam, MA, PhD, MIMM

Geophysics
G. S. Kimbell, BSc

London 1981

A report prepared for the Department of Industry

Mineral Reconnaissance Programme Reports

1 The concealed granite roof in south-west Cornwall

2 Geochemical and geophysical investigations around Garras Mine, near Truro, Cornwall

3 Molybdenite mineralisation in Precambrian rocks near Lairg, Scotland

4 Investigation of copper mineralisation at Vidlin, Shetland

5 Preliminary mineral reconnaissance of Central Wales

6 Report on geophysical surveys at Struy, Inverness-shire

7 Investigation of tungsten and other mineralisation associated with the Skiddaw Granite near Carrock Mine, Cumbria

8 Investigation of stratiform sulphide mineralisation in parts of central Perthshire

9 Investigation of disseminated copper mineralisation near Kilmelford, Argyllshire, Scotland

10 Geophysical surveys around Talnotry mine, Kirkcudbrightshire, Scotland

11 A study of the space form of the Cornubian granite batholith and its application to detailed gravity surveys in Cornwall

12 Mineral investigations in the Teign Valley, Devon. Part 1—Barytes

13 Investigation of stratiform sulphide mineralisation at McPhun's Cairn, Argyllshire

14 Mineral investigations at Woodhall and Longlands in north Cumbria

15 Investigation of stratiform sulphide mineralisation at Meall Mor, South Knapdale, Argyll

16 Report on geophysical and geological surveys at Blackmount, Argyllshire

17 Lead, zinc and copper mineralisation in basal Carboniferous rocks at Westwater, south Scotland

18 A mineral reconnaissance survey of the Doon-Glenkens area, south-west Scotland

19 A reconnaissance geochemical drainage survey of the Criffel-Dalbeattie granodiorite complex and its environs

20 Geophysical field techniques for mineral exploration

21 A geochemical drainage survey of the Fleet granitic complex and its environs

22 Geochemical and geophysical investigations north-west of Llanrwst, North Wales

23 Disseminated sulphide mineralisation at Garbh Achadh, Argyllshire, Scotland

24 Geophysical investigations along parts of the Dent and Augill Faults

25 Mineral investigations near Bodmin, Cornwall. Part 1-Airborne and ground geophysical surveys

26 Stratabound barium-zinc mineralisation in Dalradian schist near Aberfeldy, Scotland: Preliminary report

27 Airborne geophysical survey of part of Anglesey, North Wales

28 A mineral reconnaissance survey of the Abington-Biggar-Moffat area, south-central Scotland

29 Mineral exploration in the Harlech Dome, North Wales

30 Porphyry style copper mineralisation at Black Stockarton Moor,south-west Scotland

31 Geophysical investigations in the Closehouse-Lunedale area

32 Investigations at Polyphant, near Launceston, Cornwall

33 Mineral investigations at Carrock Fell, Cumbria. Part 1-Geophysical survey

34 Results of a gravity survey of the south-west margin of Dartmoor, Devon

35 Geophysical investigation of chromite-bearing ultrabasic rocks in the Baltasound-Hagdale area, Unst, Shetland Islands

36 An appraisal of the VLF ground resistivity technique as an aid to mineral exploration

37 Compilation of stratabound mineralisation in the Scottish Caledonides

38 Geophysical evidence for a concealed eastern extension of the Tanygrisiau microgranite and its possible relationship to mineralisation

39 Copper-bearing intrusive rocks at Cairngarroch Bay, south-west Scotland

40 Stratabound barium-zinc mineralisation in Dalradian schist near Aberfeldy, Scotland: Final report

41 Metalliferous mineralisation near Lutton, Ivybridge, Devon

42 Mineral exploration in the area around Culvennan Fell, Kirkcowan, south-western Scotland

43 Disseminated copper-molybdenum mineralisation near Ballachulish, Highland Region

The Institute of Geological Sciences was formed by the incorporation of the Geological Survey of Great Britain and the Geological Museum with Overseas Geological Surveys and is a constituent body of the Natural Environment Research Council

Bibliographical reference
Haslam, H. W. and Kimbell, G. S. 1981. Disseminated copper-molybdenum mineralisation near Ballachulish, Highland Region
Mineral Reconnaissance Programme Rep. Inst. Geol. Sci., No. 43

Typeset and photocopied in England for the Institute of Geological Sciences by Imediacom Ltd

CONTENTS

FIGURES

TABLES

SUMMARY

Chalcopyrite-pyrite-molybdenite mineralisation, in disseminated, veinlet and fracture-filling forms, is developed in adamellite and microadamellite in the Ballachulish igneous complex. Minor scheelite is associated with the sulphides, but is mostly confined to the adamellite. The mineralisation occurs sporadically over an area of at least 1800 x 800 m. It is best developed in and around the eastern part of the microadamellite over an area of about 250 x 450 m, where it was observed over a vertical interval of 250 m from the highest exposure to the base of a borehole. An IP survey showed that chargeability values are slightly higher in this area. The grade is variable. In 10 ft (3 m) lengths of core, the maximum Cu content was 264 ppm and the maximum molybdenum content 501 ppm, but the average tenor over the (250 x 450 m) mineralised area is not more than 50-100 ppm Cu and 10-30 ppm Mo. Selected mineralised outcrop samples gave values of up to 2386 ppm Cu, 9257 ppm Mo, 2434 ppm W, 0.31 ppm Au and 8 ppm Ag. Rb-Sr isotopic studies indicate that the ore minerals were deposited shortly after emplacement of the host rocks, and it is considered that they were introduced by a hydrothermal system which, compared with those of classic porphyry models, was small in extent and weak in intensity. Sericitic alteration is generally associated with the mineralisation, but there is no potassic alteration evident and the standard zonation of porphyry copper deposits is absent. There is very little K or Rb metasomatism, the best defined chemical change being a loss of Sr in altered rocks. The hydrothermal fluids, as seen in fluid inclusions, were of moderate salinity, unlike the high salinity fluids usually characteristic of porphyry copper deposits. Anomalously low Rb and high K/Rb values in the unaltered microadamellite are attributed to the separation of a Rb-rich aqueous fluid from the microadamellite before or at the time of consolidation of the rock. The mineralised area lies adjacent to and northwest of a NNE-trending shatter belt, which may have provided structural control at depth, although at the present level of exposure the microadamellite body appears to be the structural control.

INTRODUCTION

The Ballachulish igneous complex (Figure 1) occupies an area of rugged terrain east of Loch Linnhe about 20 km WSW of Fort William. Much of the area is devoted to forestry, the remainder being rough grazing. Access is provided by forestry roads leading off the A828.

The presence of copper-molybdenum mineralisation in the main stream section in Gleann a' Chaolais was recorded by Evans (1977), who concluded from his preliminary observations that exploration in depth might be rewarding. A more detailed surface investigation was carried out under the Mineral Reconnaissance Programme in 1978, followed by the drilling of a borehole in 1979. Because of his earlier studies, Dr. A.M. Evans of the Department of Geology at Leicester University collaborated with IGS, principally by extending his earlier fluid inclusion studies to a wider suite of samples (see Evans and others, 1980).

GEOLOGY AND MINERALISATION

The Ballachulish igneous complex was intruded into Dalradian schists, quartzites and limestones, and thermal metamorphic effects in these country rocks have been described (Bailey and Lawrie, 1960). Read (1961) placed the granite in the category of Forceful Newer Granites, along with Rogart, Strontian and Moor of Rannoch, all considered to be of late Silurian or early Devonian age, and recent classifications have broadly confirmed this setting for Ballachulish (e.g. Simpson and others, 1979; Plant and others, 1980).

Miller and Brown (1965) and Brown and others (1968) gave four K-Ar mineral ages for the Ballachulish complex: 405 ± 18, 395 ± 18, 420 ± 19 and 387 ± 6 Ma. An age of 410 Ma was assumed by Harmon and Halliday (1980) in calculating initial $^{87}Sr/^{86}Sr$ ratios of 0.70424 and 0.70433 for two samples from the northwest of the complex.

The pluton was divided by Lawrie into an early quartz diorite or tonalite and a later, mostly central, pink granite (on the 1 inch Geological Sheet 53, and in the descriptive memoir by Bailey and Lawrie, 1960). More detailed studies by Muir (1950) showed the central, more siliceous rock to be adamellite and the outer zone to consist of granodiorite in the north, quartz diorite in the south, and pyroxene mica diorite in the east (Figure 1). The mineralisation described in this report is confined to the adamellite (following Muir's nomenclature) and a small central body of leucocratic microadamellite (Evans and others, 1980).

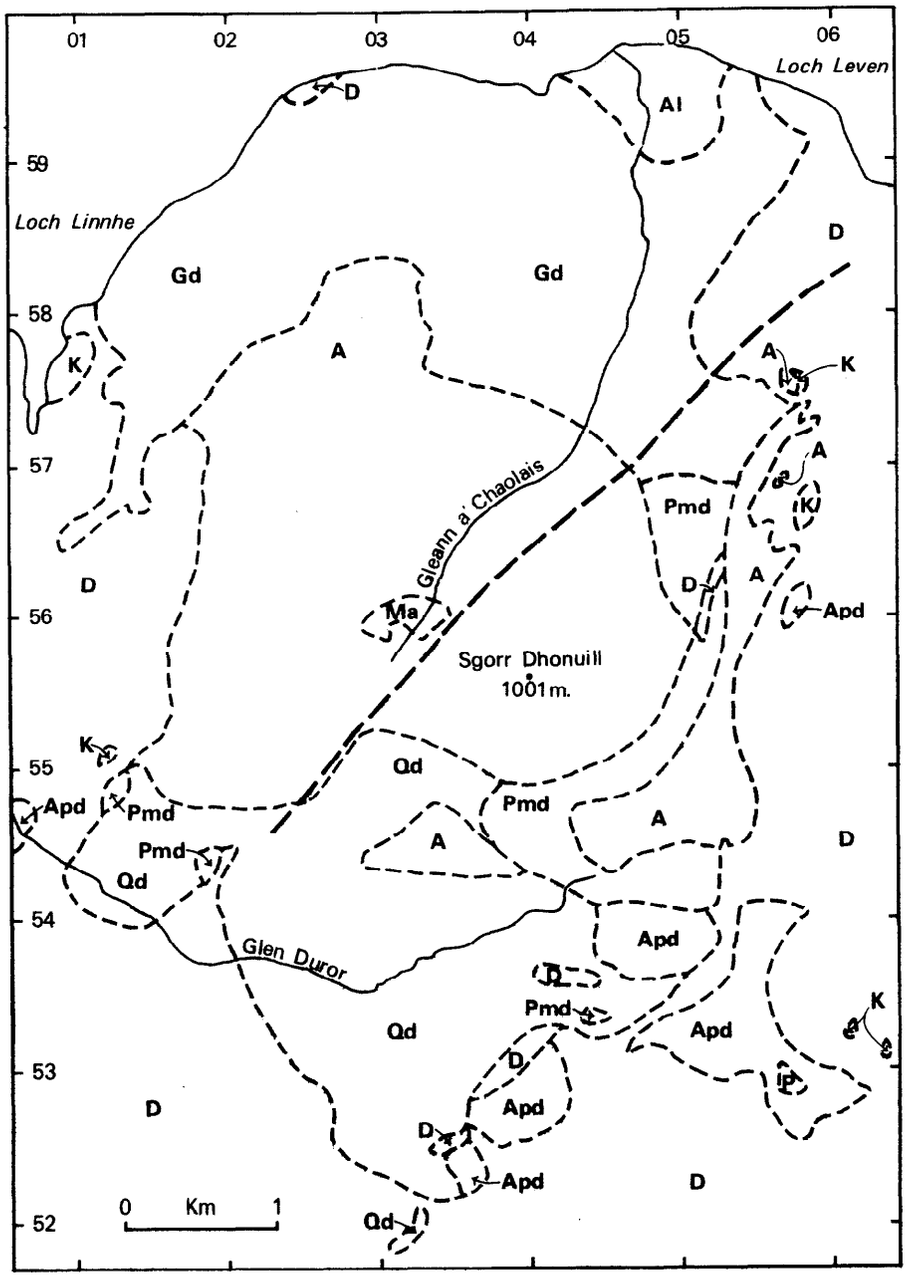

Al	Alluvium	Apd	Appinitic diorite
Ma	Microadamellite	K	Kentallenite
A	Adamellite	P	Peridotite
Gd	Granodiorite	D	Dalradian
Qd	Quartz diorite	----	Geological boundary
Pmd	Pyroxene mica diorite	——	Shatter belt

Fig.1. Ballachulish igneous complex.
Geological information mainly from Muir (1950), with additions from the geological map (Sheet 53) and from the present study.

ADAMELLITE

The adamellite is fairly uniform in mineralogical composition, though some minor variations are apparent. Plagioclase is in the range oligoclase to andesine, and is normally zoned. Sericitic alteration is common; cores of crystals are generally more affected than margins, but this effect is often overshadowed by an irregular patchiness of the alteration. Orthoclase is less altered. Microperthitic texture is poorly developed, and some of the larger crystals are zoned. Brown biotite is partly altered to chlorite, but green hornblende is fresh, Clinopyroxene is present in some specimens, and is partly replaced by hornblende. Apatite, sphene and opaques occur as accessory minerals. Infrequent minor shears are found in the adamellite within the mineralised area, in addition to the larger shatter belt described below.

MICROADAMELLITE

The outcrop of the microadamellite measures about 650 m x 250 m and is entirely surrounded by the adamellite (Figure 2). Some exposures show a sharp contact between the two rock types, but elsewhere there appears to be a merging junction. No chilled margin or metamorphic effects were noted. The microadamellite outcrops chiefly in the valley of the Abhainn Greadhain but it extends westwards almost to the top of the ridge. The intersection of the northern contact with the slopes of the valley suggests that the contact may have a northerly dip of 45°, though it is also possible that the contact is vertical or has some other angle of dip and that a bend in the line of the contact coincides with the point where it crosses the Abhainn Greadhain. The eastern part of the microadamellite is affected by quartz veining and mineralisation, but the western part is not.

The microadamellite is a leucocratic rock with small and variable amounts of chlorite (after biotite), opaque minerals and rare surviving biotite. Quartz is abundant and plagioclase and alkali feldspar are present in approximately equal proportions. The rock thus merits the name microadamellite, on the basis of its mineralogy, although its chemical composition (Table 3) is more typical of a granite than an adamellite. The plagioclase is oligoclase, sometimes with slight zoning. As in the adamellite, it shows patchy alteration to sericite. Alteration products of the orthoclase microperthite are sericite, carbonate and, locally, kaolinite, though alteration is generally less intense than in the plagioclase. In some specimens muscovite appears to be, in part, a primary mineral, but mostly this mineral is secondary, as a replacement of feldspar and as a pseudomorph (with magnetite, ilmenite, hematite and/or chlorite) after biotite. In addition to the opaque oxides, apatite occurs as an accessory mineral.

DYKES

A few dykes of intermediate composition (recorded as microdiorite on Figure 2) occur in and near the mineralised area. They are fine grained, some very fine grained. Plagioclase and quartz are identifiable in some dykes, but others consist entirely of secondary minerals such as sericite, carbonate and chlorite.

One dyke which resembles the microadamellite is shown on Figure 2.

Aplites occur rarely within the microadamellite, composed of quartz and alkali feldspar with a little plagioclase, muscovite and iron oxides.

SHATTER BELT

The complex is crossed by a NNE-trending shatter belt which is marked on the one inch geological map, sheet 53, at [Grid Reference NN 055 580] and was recorded by Muir (1950) in the vicinity of [NN 028 552] where it displaces the southern margin of the adamellite. In the present study its course was traced by outcrop evidence and by geophysical means (see p. 6) in the upper part of Gleann a' Chaolais (Figure 2) where it passes to the southeast of the microadamellite. Rock samples collected from near the shatter belt (e.g. XDR 75, 135 and 154, Table 2) show quartz veining and strong hydrothermal alteration (sericitisation of feldspars and chloritisation of biotite). Some samples are granulated (e.g. XDR 135) but most show no evidence of deformation. The style of alteration differs from that associated with the mineralisation (see below), principally in the survival of chlorite (and, in XDR 75, hornblende cored by clinopyroxene) in strongly altered rocks.

To the north, the shatter belt is probably continuous with the major shatter belt which has been traced from Callert, north of Loch Leven, [NN 117 616] northeastwards to Tulloch in Glen Spean (Johnstone, 1954, 1966). The southward continuation has not been traced with certainty. Immediately northwest and southeast of the pluton, the belt runs close to (c.100 m southeast of) the earlier Ballachulish-Benderloch slide (Bailey and Lawrie, 1960; Litherland, 1980), a low angle thrust with no structural significance at depth.

MINERALISATION

Sulphide mineralisation (Evans, 1977; Evans and others, 1980) occurs in the upper part of the Gleann a' Chaolais. The geographical extent is illustrated by the map of Cu in bedrock, Figure 15. Sulphide minerals occur sporadically over an area of at least 1800 x 800 m, but they are best developed in and around the eastern part of the microadamellite, in an area of about 250 x 450 m, between 400 m and 550 m altitude (Figure 16), within which mineralised quartz veinlets and disseminated sulphides are particularly common.

The richest observed example of a mineralised

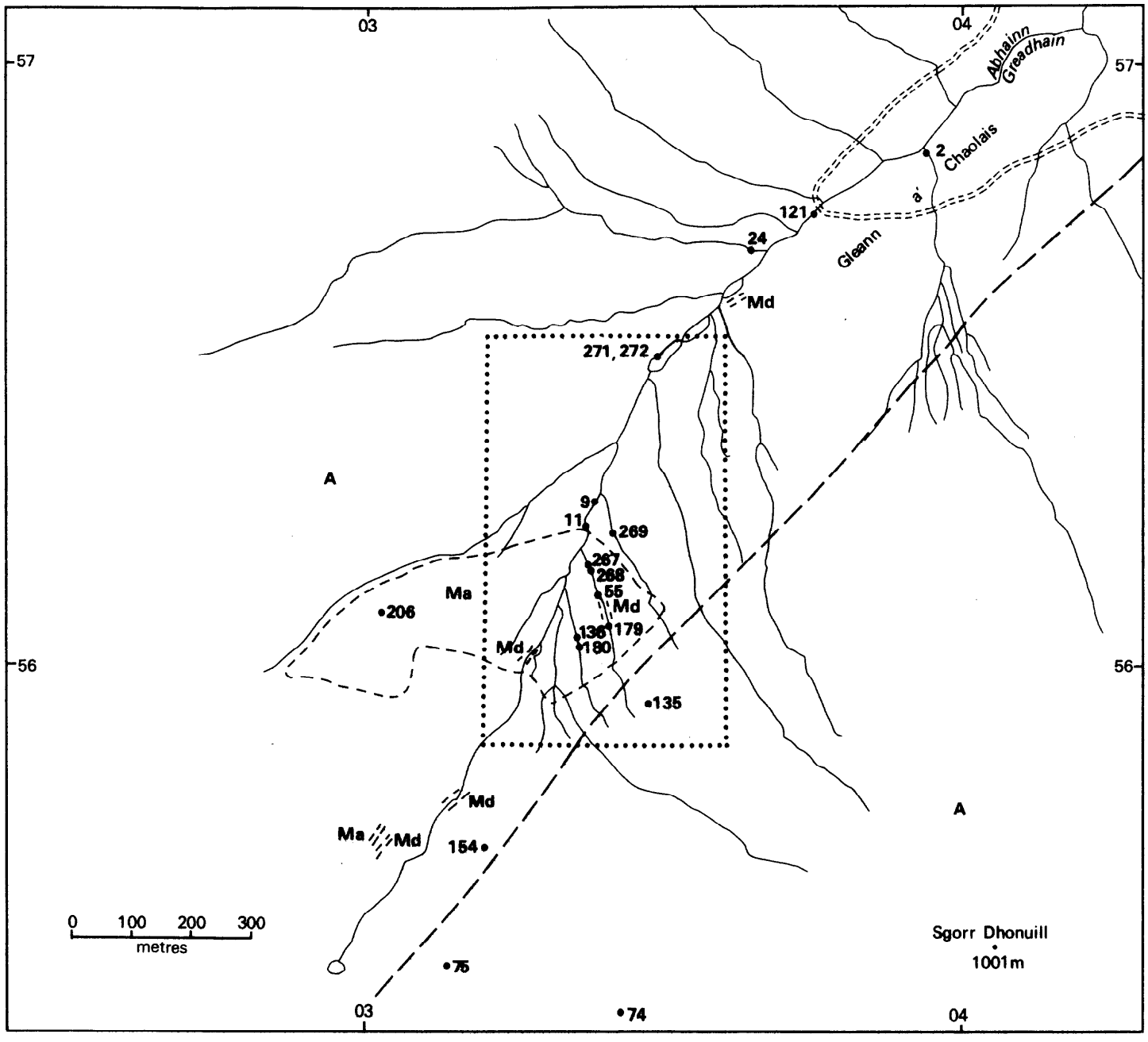

Md Microdiorite

Ma Microadamellite

A Adamellite

Geological boundary

Shatter belt (approximate)

Forest road

Outline of Figs. 16 and 18

11• Outcrop sample locality, with XDR sample number (see Tables 2,3 and 4)

Fig.2 Geological map of central part of Ballachulish complex, showing selected outcrop sample localities.

vein lines outside this inner area, at [NN 0348 5651] (Table 4, samples XDR 271 and 272). It is a 1 cm wide vein, which, with other associated veins and veinlets, contains abundant chalcopyrite and molybdenite, as well as some scheelite. It is near-vertical and may be traced in outcrop for a few metres, with an east-west trend.

Some samples from in and near the shatter belt are mineralised, but the main mineralised localities lie northwest of the belt, and the mineralisation appears to be associated spatially and structurally more with the microdamellite than with the shatter belt.

The most abundant ore minerals are pyrite, chalcopyrite and molybdenite, occurring in quartz veinlets, as fracture coatings, and as disseminations. Bornite has been noted in borehole core (Appendix I), both as a disseminated phase and in quartz veinlets. Goethite and malachite are secondary minerals, and covellite rarely forms a thin rim around chalcopyrite and bornite grains. Tetrahedrite, which was recorded by Evans (1977), was not observed in the present study. Scheelite forms whitish crystals in and near quartz veinlets. It is very rare in the microadamellite, but less so in mineralised adamellite. It fluoresces pale cream in ultraviolet radiation, which indicates the presence of Mo. Trace arsenopyrite was noted in one core sample.

Most of the more persistent mineralised veins, veinlets and fractures have an east-west trend and a steep northerly dip. Veinlets with other trends do occur but are not common. Further details of the style of mineralisation are given in the borehole log (Appendix I). Each of the main ore minerals frequently occurs independently of the others, but this does not prove that they represent different phases of mineralisation and indeed the ore minerals often occur in association, both in quartz veinlets and in disseminations. The straight-edged mineralised veinlets and fractures perpendicular to the core length are cut by (and therefore precede) the more irregular features (e.g. calcite veinlets; fractures coated with chlorite or dioctahedral mica). The fractures coated with fine-grained molybdenite (e.g. at 31.1 to 31.4 m in the core) appear to belong to the later period of activity; this may represent a second phase of molybdenum mineralisation, or it may indicate remobilisation of earlier molybdenite.

ALTERATION

Hydrothermal alteration, of the styles described above, is widespread in and around the mineralised area (Evans and others, 1980). Alteration effects tend to be more intense, in general, within the areas in which sulphide mineralisation is best developed and, more specifically, in individual mineralised specimens from within and outside these restricted areas. Exceptions may be found, however, and some mineralised samples, from within and outside the areas of best developed mineralisation, show a low intensity of alteration.

Evans and others (op. cit.) described low, medium and high intensities of alteration. Samples with a low intensity are rare in the microadamellite and occur typically in the adamellite in areas peripheral to the mineralisation (e.g. XDR 2, 11, 24, 74, 121 in Table 2 and Fig. 2). The feldspars are weakly sericitised, biotite and hornblende are partially chloritised, and calcite and epidote are occasionally present. A medium intensity of alteration is characteristic of the microadamellite (e.g. XDR 136, 206 in Table 3), with plagioclase more sericitised and biotite entirely replaced by chlorite with or without sericite. Carbonate may be present. In the adamellite the alteration is similar, and in addition hornblende has mostly been replaced by chlorite and epidote is now absent; this medium-intensity alteration is found in and near mineralisation (e.g. XDR 9 in Table 2 and XDR 269 in Table 4). At a high intensity of alteration, restricted to mineralised samples in both rock types, sericite and carbonate persist but chlorite is absent (e.g. XDR 179, 180 in Table 3, XDR 267, 268, 271 in Table 4).

The presence of intensely sericitised rocks associated with the mineralisation and of chlorite, calcite and epidote in the more weakly altered rocks, especially those peripheral to the more highly altered rocks, led Evans and others (op. cit.) to conclude "The mineralisation is associated with phyllic alteration of the host rocks and there is some evidence for the possible pre-existence of propylitic alteration", but the well-defined zoning of alteration which is characteristic of porphyry copper deposits elsewhere is absent at this locality.

The principal alteration effects in these rocks (a reddening of the feldspars, and the development of white mica, chlorite, calcite and kaolinite at the expense of higher temperature minerals) can take place in association with (1) plutonic processes (hydrothermal alteration during cooling) (2) deformation (hydrothermal alteration during shearing), (3) mineralisation, or (4) weathering. In the area under study, weathering is restricted to the superficial crust and is not an important cause of the alteration effects described in the rocks. In the main shatter belt and in other sheared specimens, hydrothermal alteration is clearly associated with deformation. Most of the alteration described is, however, clearly associated either with late-stage magmatic processes or with mineralisation. The spatial association with mineralisation and with a high density of fluid inclusions (Evans and others, op. cit.) is strong evidence for attributing much of the alteration to the action of the mineralising fluids, although minor sericitisation and alteration is much more widespread than the mineralisation and is likely to have taken place at the magmatic stage.

GEOPHYSICS

METHODS

Induced polarisation (IP) and resistivity measurements were made along a set of NW-SE survey lines (Figure 3) using Huntec Mk. III time domain equipment. Both pyrite and chalcopyrite are good conductors (molybdenite is only a moderate conductor) and disseminated conductive mineralisation will give an IP response if present in sufficient concentrations, although not necessarily affecting the bulk resistivity of the rock. A water-filled shatter belt should have a lower bulk resistivity than neighbouring solid rock.

'Chargeabilities', which give a measure of the IP effect, were derived from the time integral of the voltage decay curve between 240 and 1140 millisecs after switching off a 2 second current pulse. A colinear dipole-dipole electrode configuration was adopted with 50 m dipoles and dipole centre separations of 100 m (n = 2) to 300 m (n = 6). Dipole lengths were measured parallel to the ground surface to allow comparison of results from the steep but relatively uniform slopes with those from flatter areas. To avoid ambiguity, all electrode positions are marked on the figures.

RESULTS AND DISCUSSION

Results from the dipole dipole traverses are presented as contoured pseudosections (Figures 4 to 9). Using Edwards' (1977) coefficients for 'effective depth', the greatest depth of investigation achieved in this survey is very approximately 75 m (at the n = 6 dipole separation).

Apparent resistivities are fairly variable, ranging from about 1000 to 40000 ohm m. Some of the variations may be artificial since topography alone can produce apparent resistivity (but not IP) anomalies. Over ground of uniform true resistivity an apparent resistivity pseudosection across a concave change in slope (e.g. a valley bottom) will show a central low flanked by zones of higher apparent resistivity while a convex slope change will produce the opposite pattern—a central high flanked by lows (Fox and others, 1980). Topographic profiles accompany the pseudosections to help distinguish the causes of anomalies. For example, on line 200 NE a resistivity low centred at 675 SE is probably of topographic origin while the more striking resistivity low around 1000 SE is not associated with such a marked change in slope (Figure 6). The latter anomaly appears to be due to a shatter belt known to occur in this vicinity and the contour map of apparent resistivity at the n = 3 dipole separation (Figure 10a) shows the roughly northeasterly trend of this anomalous zone. Lower apparent resistivities are also found on the northwest side of the survey area in a rather more diffuse ENE trending zone which is unlikely to be of topographic origin and which possibly indicates a region of greater fracturing.

The metal fences in this area probably do not have a great influence on apparent resistivities but, when grounded, they can cause strong IP anomalies (Nelson, 1977). For example, the correlation of an anomalous zone with the fence on the west side of the survey area is evident in Figure 10b. The strength of the response varies along the fence because of changes in the frequency of grounding points and in the grounding impedance. It is possible that artificial anomalies could overlie and obscure genuine ones.

Away from the influence of fences. chargeabilities are low (generally less than 10 millisecs). The background level is probably influenced by membrane effects in clay minerals in the overburden and there is a tendency for lower (and sometimes negative) values to occur over the higher slopes where overburden is very thin.

There is no geophysical evidence to suggest a concentration of mineralisation in the shatter belt. Chargeabilities actually tend to be lower over this belt, although this may be because current tends to be channelled along more conductive water filled fissures rather than through the rock.

Slightly higher chargeability values (up to 10.9 ms) are found where line 100 NE crosses the area of most conspicuous observed mineralisation and these appear to be genuine as they arise from electrode arrays which do not span the fences (Figure 5). There is evidence of possibly two, fairly shallow mineralised zones with no indication of increasing mineralisation with depth. The borehole passes through the anomalous region beneath line 100 NE and the log (see p. 39 and Figure 24) shows higher chargeabilities at shallow depths, agreeing with the results of the ground survey. It is possible that the two distinct high chargeability zones in the log correlate with the two in the pseudosection but there is insufficient evidence to confirm this with any certainty.

Genuine chargeabilities of greater than 8 ms occur in the centre of line 200 NE (Figure 6), around 625 NW and 400 NW on line 500 NE (Figure 8) and at the southeast end of line L2 (Figure 9). These may indicate slightly higher concentrations of conductive minerals but there is no indication of appreciable mineralisation.

DRAINAGE GEOCHEMISTRY

Panned concentrate samples were collected from 47 sites, and 100 mesh stream sediments from 44 sites. Both sets of samples were analysed by XRF for Ce, Ba, Sb, Sn, Pb, Zn, Cu, Ca, Ni, Fe, Mn, Ti, U, Sr, Zr and Mo. The results are summarised in Table 1 and the higher Cu and Mo values are plotted in Figures 11 and 12. Within the Gleann a' Chaolais catchment, the main area of copper-molybdenum mineralisation is characterised by above-background Cu and Mo values (best shown by the stream sediment results), Enhanced levels of these elements also occur to the east and NNE of the mineralised area, but the ground upstream of these sample sites

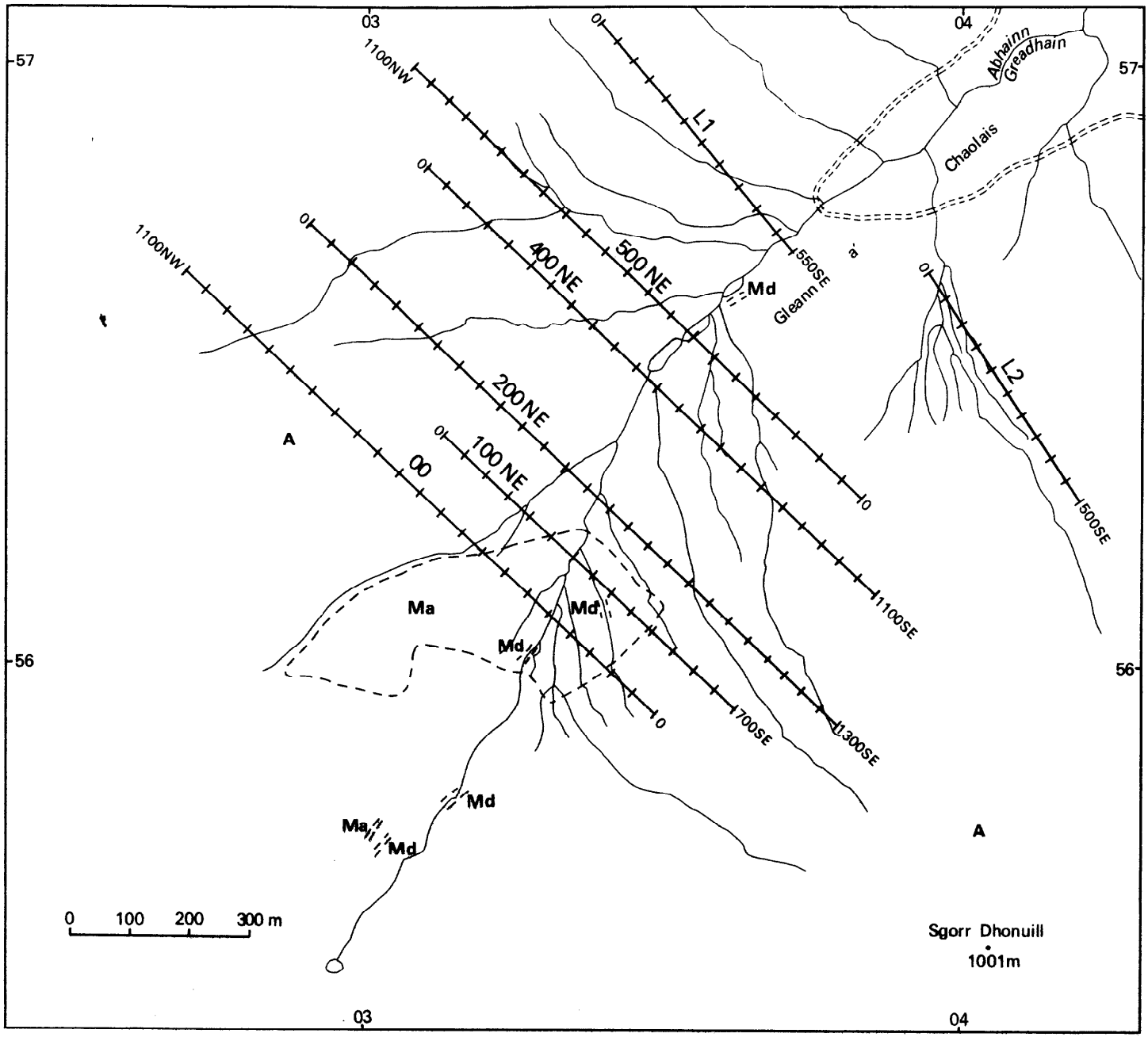

Md Microdiorite

Ma Microadamellite

A Adamellite

Geological boundary

Forest road

Geophysical traverse line showing electrode positions

Fig.3. Location of geophysical observations

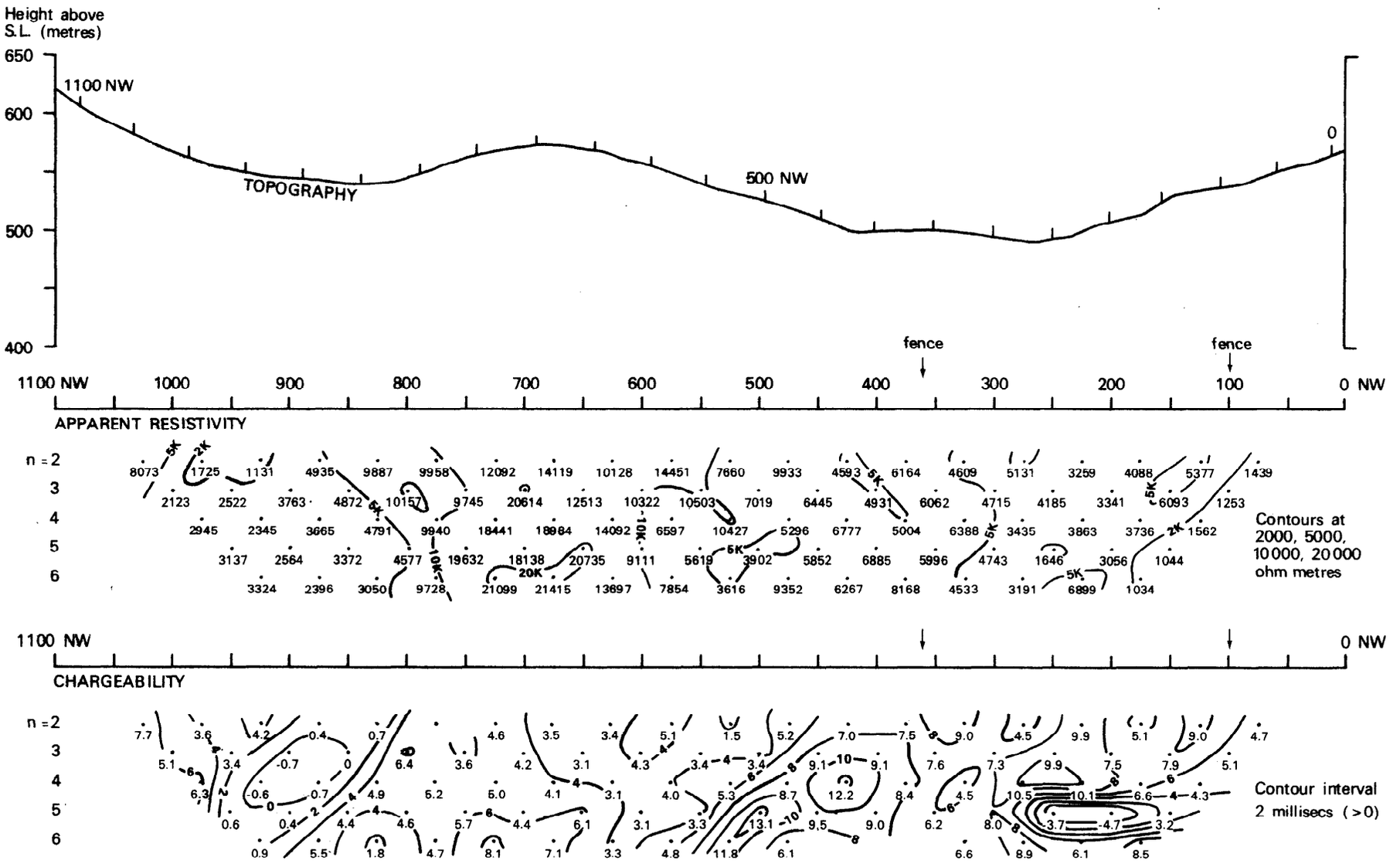

Fig. 4. Line 00 : geophysical results and topography

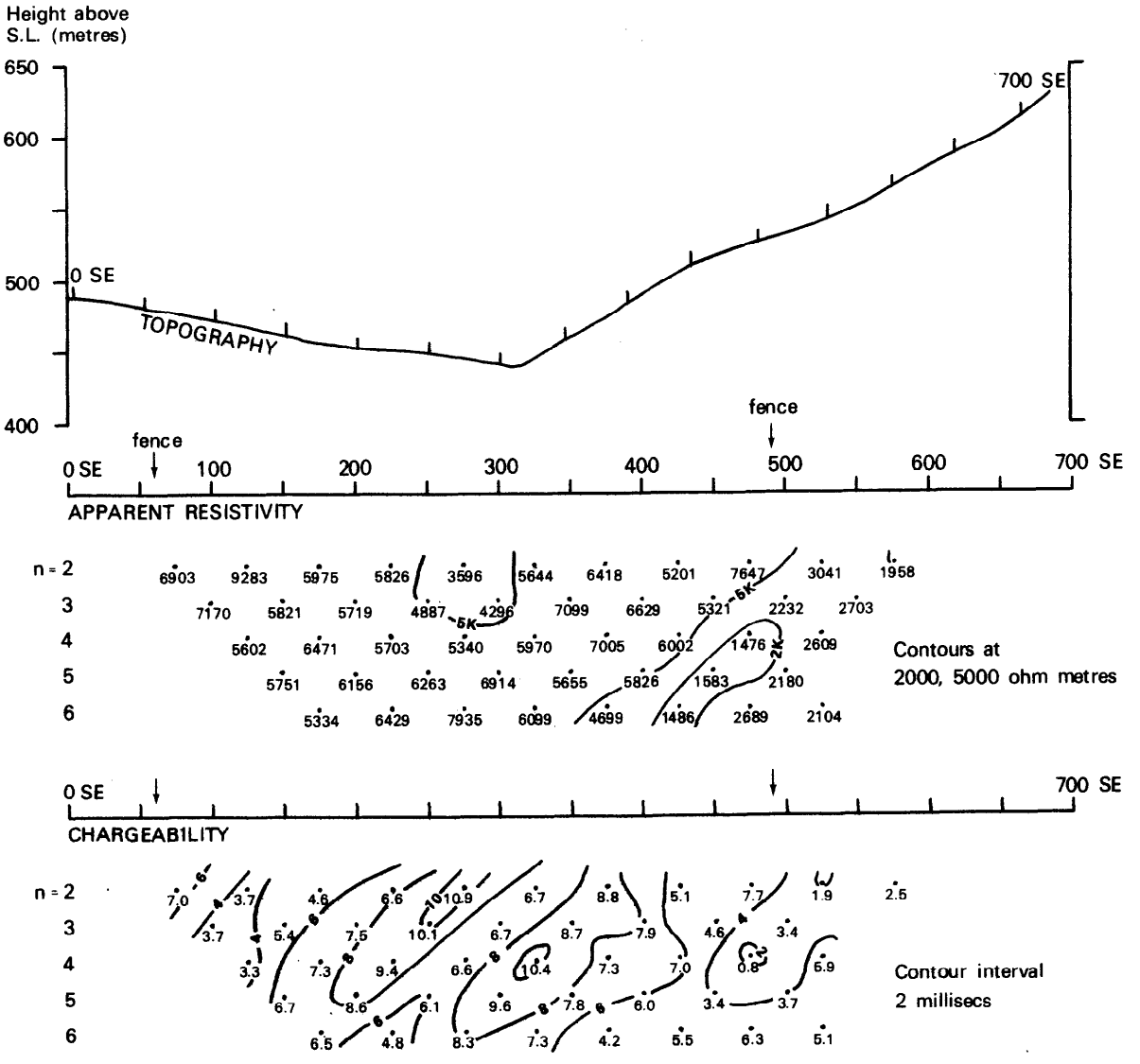

Fig. 5. Line 100 NE : geophysical results and topography

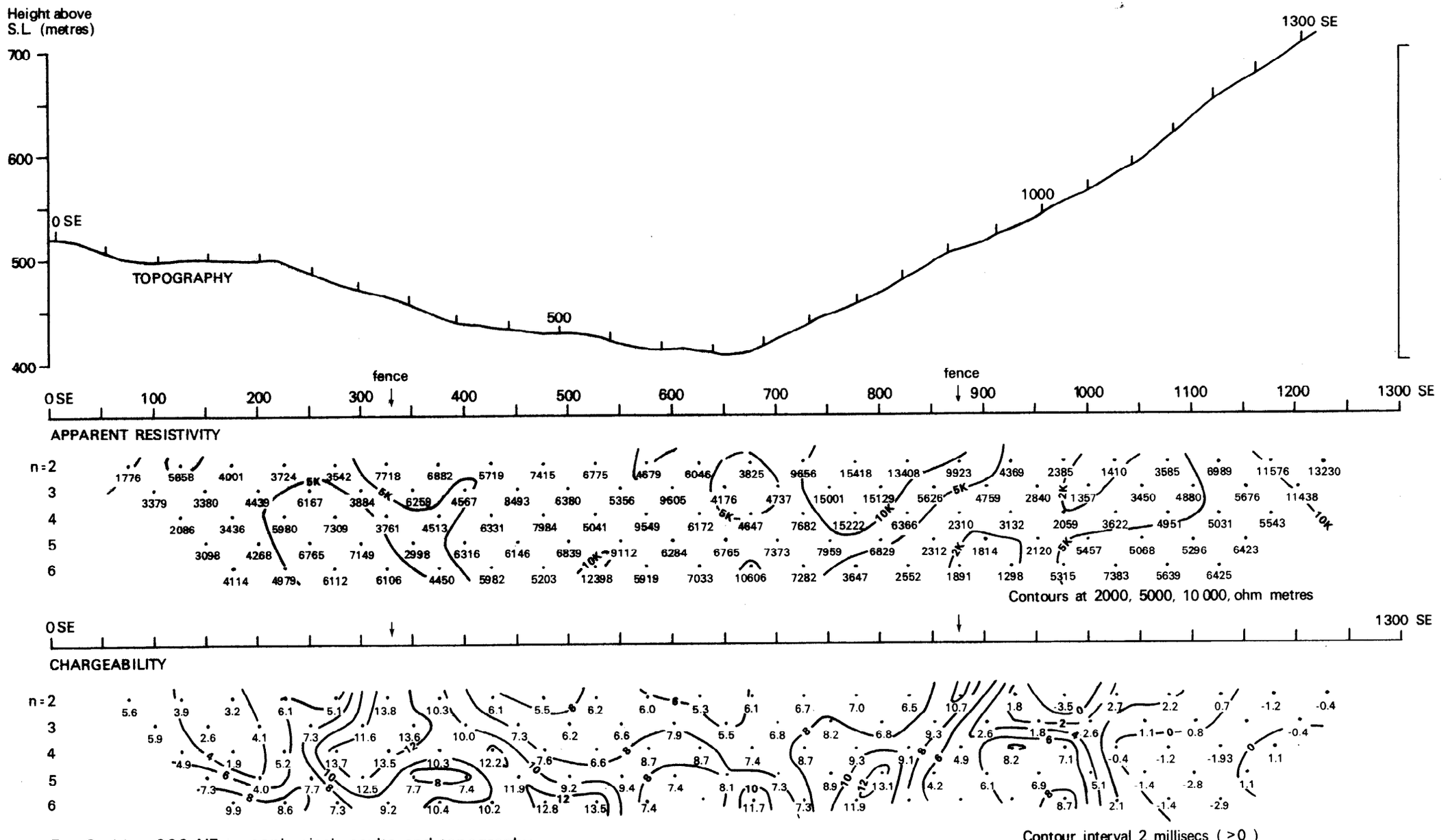

Fig. 6. Line 200 NE : geophysical results and topography

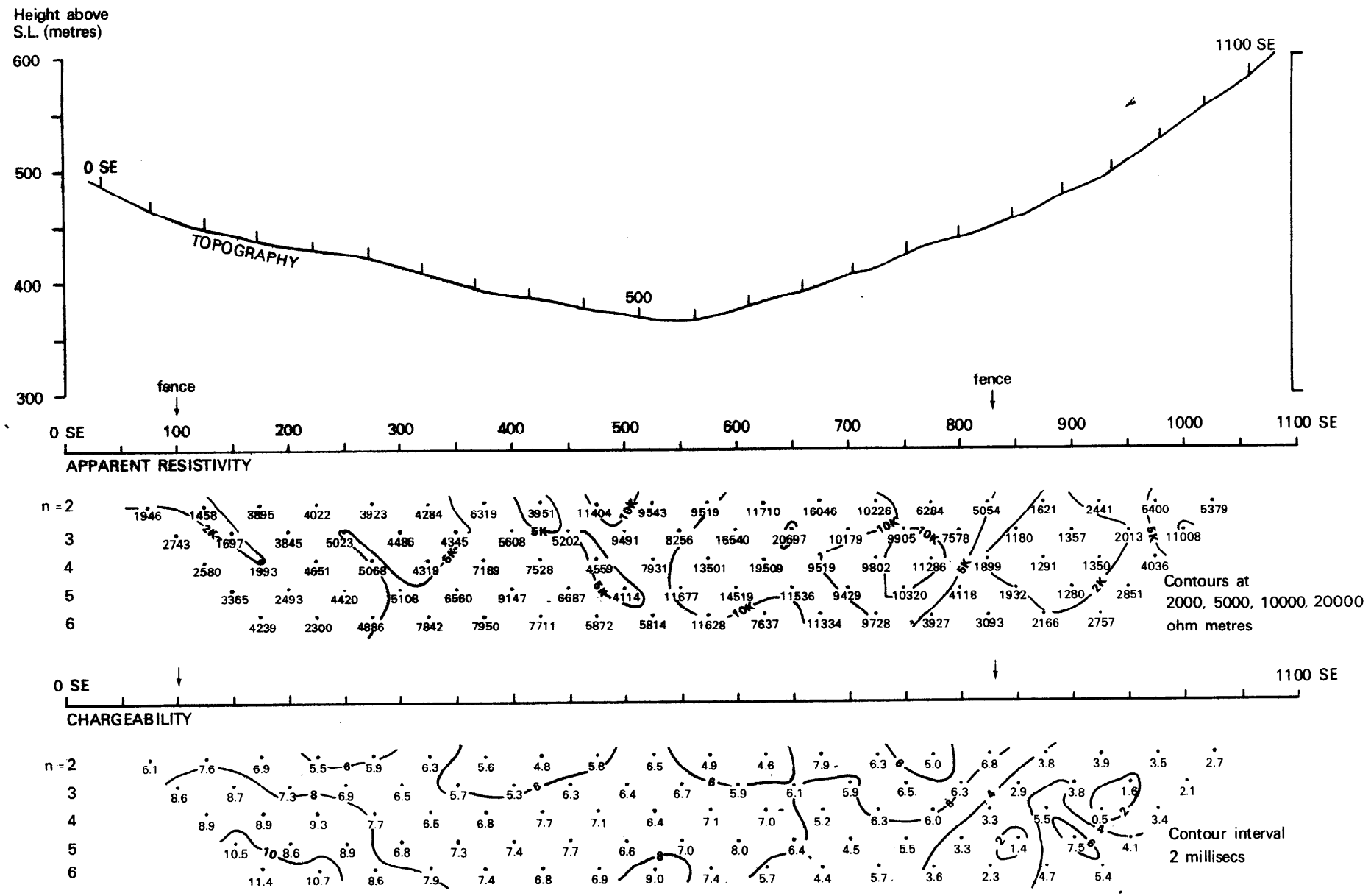

Fig.7. Line 400 NE : geophysical results and topography

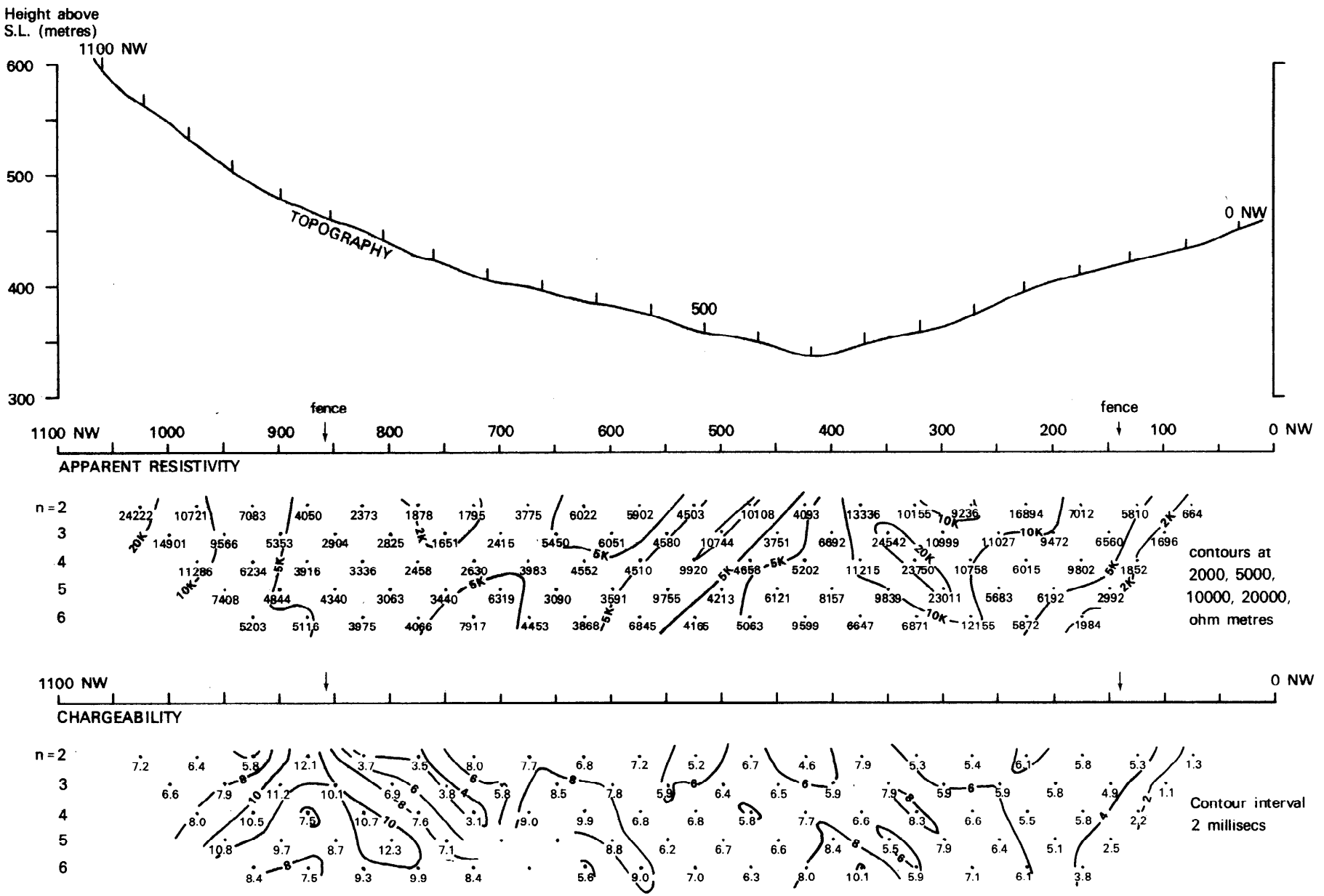

Fig. 8. Line 500 NE : geophysical results and topography

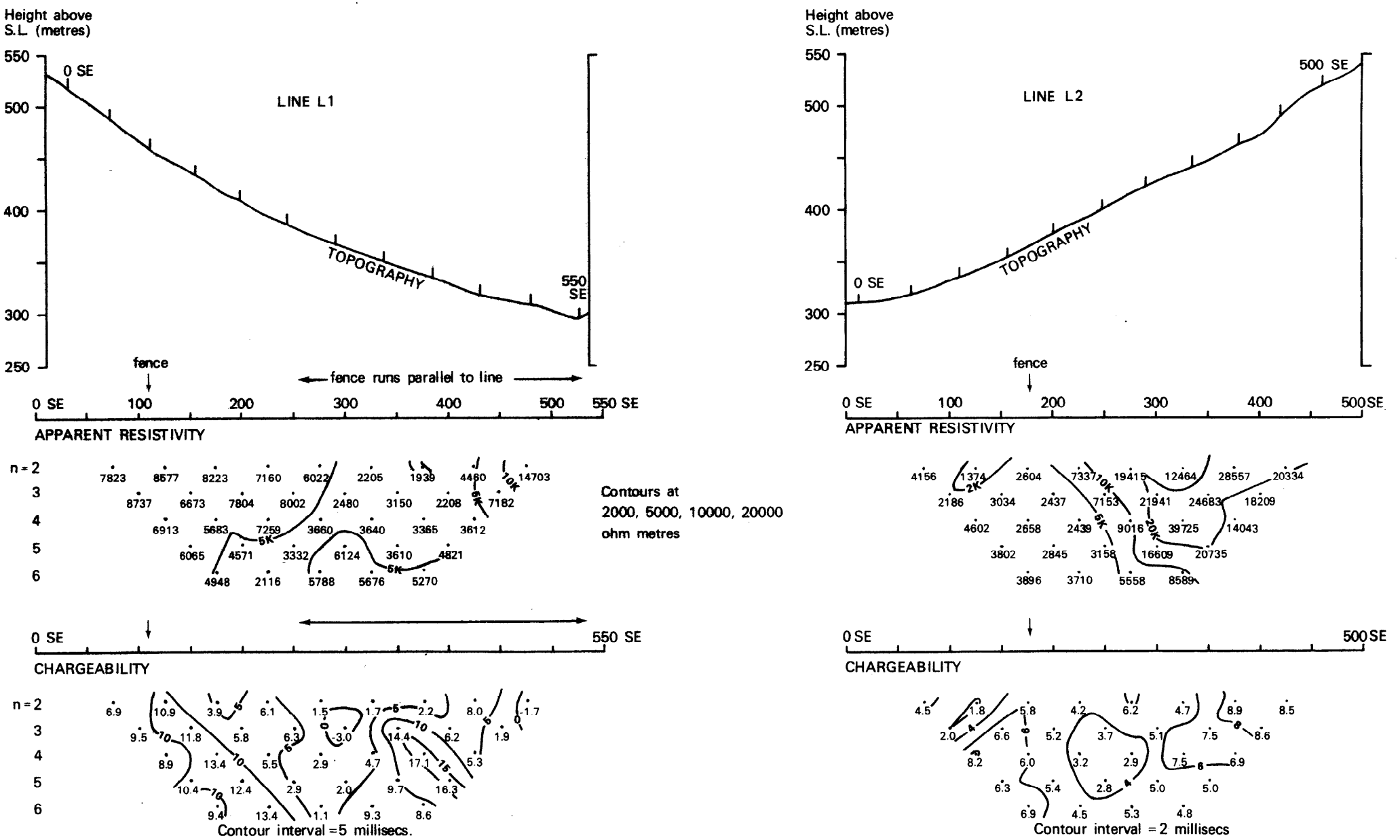

Fig. 9. Lines L1 and L2 : geophysical results and topography

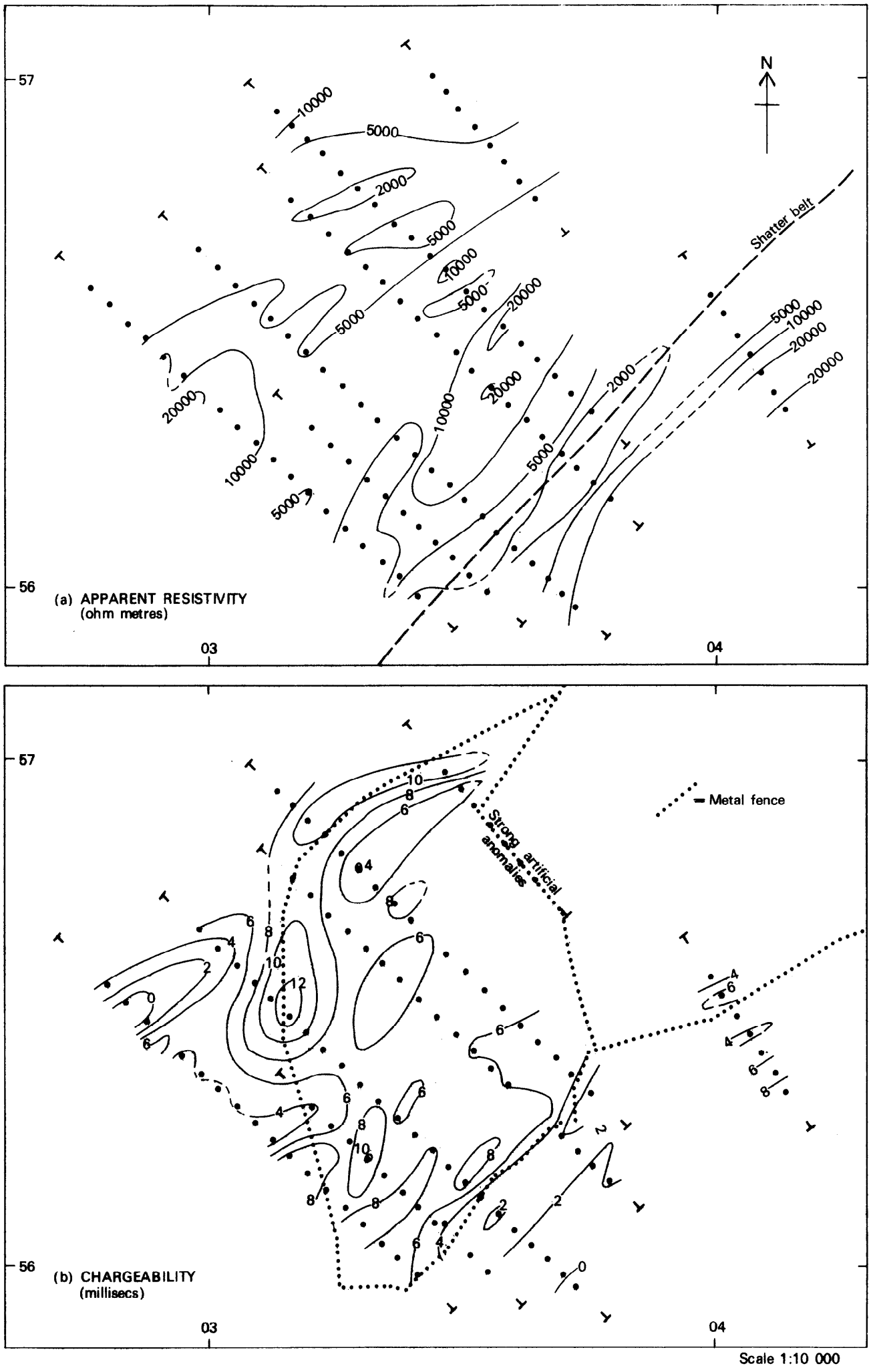

Fig. 10 Contour maps of apparent resistivity and chargeability (n=3)

Table 1 Summary statistics for 44 stream sediment and 47 panned concentrate samples

	44 stream sediments			47 panned concentrates		
	Min.	Max.	Median	Min.	Max.	Median
Ce	45	176	88	20	533	85
Ba	335	959	770	149	1053	502
Sb	<7	16	<7	<7	7	<7
Sn	<6	9	<6	<6	34	<6
Pb	20	89	41	<9	48	19
Zn	32	290	132	12	170	83
Cu	14	94	33	<3	187	12
Ca (%)	0.28	4.09	1.69	0.14	7.57	2.60
Ni	5	184	44	3	159	68
Fe (%)	2.19	9.01	6.01	1.24	16.34	7.16
Mn	390	1920	1045	100	5630	1090
Ti (%)	0.36	1.18	0.62	0.16	5.63	0.72
U	<4	140	10	<4	10	<4
Sr	70	1040	560	70	950	510
Zr	250	2200	865	200	6360	640
Mo	<2	18	4	<2	17	4

All values in ppm except where otherwise indicated.

has not been examined and the source of the Cu and Mo is not known. The northern tributary of the River Duror which shows high Cu values in both sample types [0205 5450] flows along the line of the shatter belt, and some Cu mineralisation associated with the shatter may therefore be suspected. The high Cu values in sediments in the western tributary of Allt Eilidh may be attributed to the presence of appinitic diorite and peridotite in the catchment.

Uranium values in stream sediment are high in upper part of the Gleann a' Chaolais, in and near the mineralised area, where the 14 samples show a range of 10–140 ppm U and a median of 35 ppm. The highest values are 140 ppm at [0395 5675] and 120 ppm at [0330 5630]. The source of the U was not traced, but those rock samples which have been analysed for U contain <15 ppm U (Tables 4 and 11).

ROCK GEOCHEMISTRY

SAMPLES ANALYSED FOR MAJOR AND TRACE ELEMENTS

Fourteen outcrop samples were selected for whole-rock silicate analysis. Their localities are shown on Figure 2. Major, minor and trace element data are given in Tables 2 and 3 and plotted in Figures 13 and 14. SiO_2, TiO_2, Al_2O_3, total Fe, MgO, CaO, P_2O_5 and F were determined by Betaprobe. FeO was determined by redox titration, and Fe_2O_3 by difference. The presence of sulphides in some samples invalidates the FeO and Fe_2O_3 results; the plots in Figure 13 suggest that iron in sulphide phases (pyrite and/or chalcopyrite) may register as Fe_2O_3. Na_2O and K_2O were determined by flame emission, Li by atomic absorption spectrophotometry, and the other elements by X-ray fluorescence spectrometry. Also plotted in Figure 13 are data from previously published analyses quoted in Bailey and Lawrie (1960): the analyses with CaO + MgO values of 8.9 are from the granodiorite, the analysis with CaO + MgO = 3.9, and probably also that with value 3.6, are from the adamellite, and the analysis with CaO + MgO = 4.1 is from the "white granite", a narrow strip of pyritiferous trondhjemite in contact with Dalradian (Figure 1) at the northwestern margin of the complex.

The four relatively fresh and unmineralised samples of adamellite have similar contents of all the elements determined. The two unmineralised samples of microadamellite have similar contents of most elements, but XDR 206 (which, unlike XDR 55, was collected from outside the mineralised area) contains higher Sr and Ba.

Five of the samples are mineralised and/or altered. Three of them contain high Cu, three have high Fe, and one has high Mo and W: these are the chemical effects of the introduction of ore minerals. The associated hydrothermal alteration was not accompanied by large changes in major element content. In particular, the K_2O contents of the mineralised and altered rocks differ little from those of the fresh samples (see also p. 30). Some trace elements, however, seem to have been mobilised during alteration. Li, Y, Sr, Ba, Pb and Th tend to be slightly lower in the altered rocks than in corresponding fresh speciments and, in the microadamellite, Rb is somewhat higher in the mineralised samples. Most of these differences are slight, and may be of no significance, but the Sr plot and the Ca/Sr plot do suggest that at least some of the rocks lost Sr during alteration and some Rb mobility is also indicated (see also p. 30). P_2O_5 does not increase with mineralisation.

The three samples from the shatter belt show

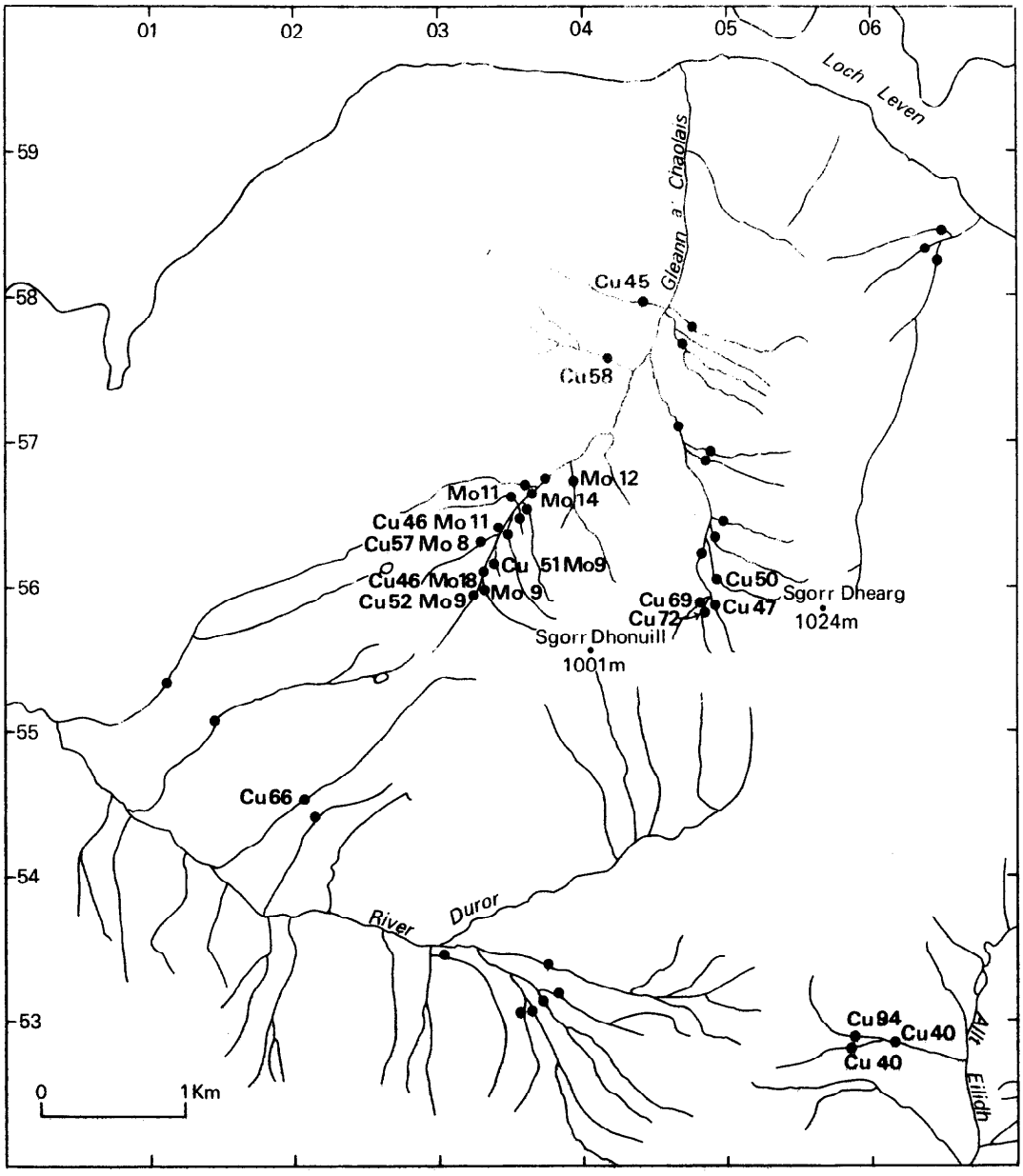

Fig. 11. Stream sediment sites, showing locations of Cu values ⩾ 40 ppm and Mo values ⩾ 8 ppm.

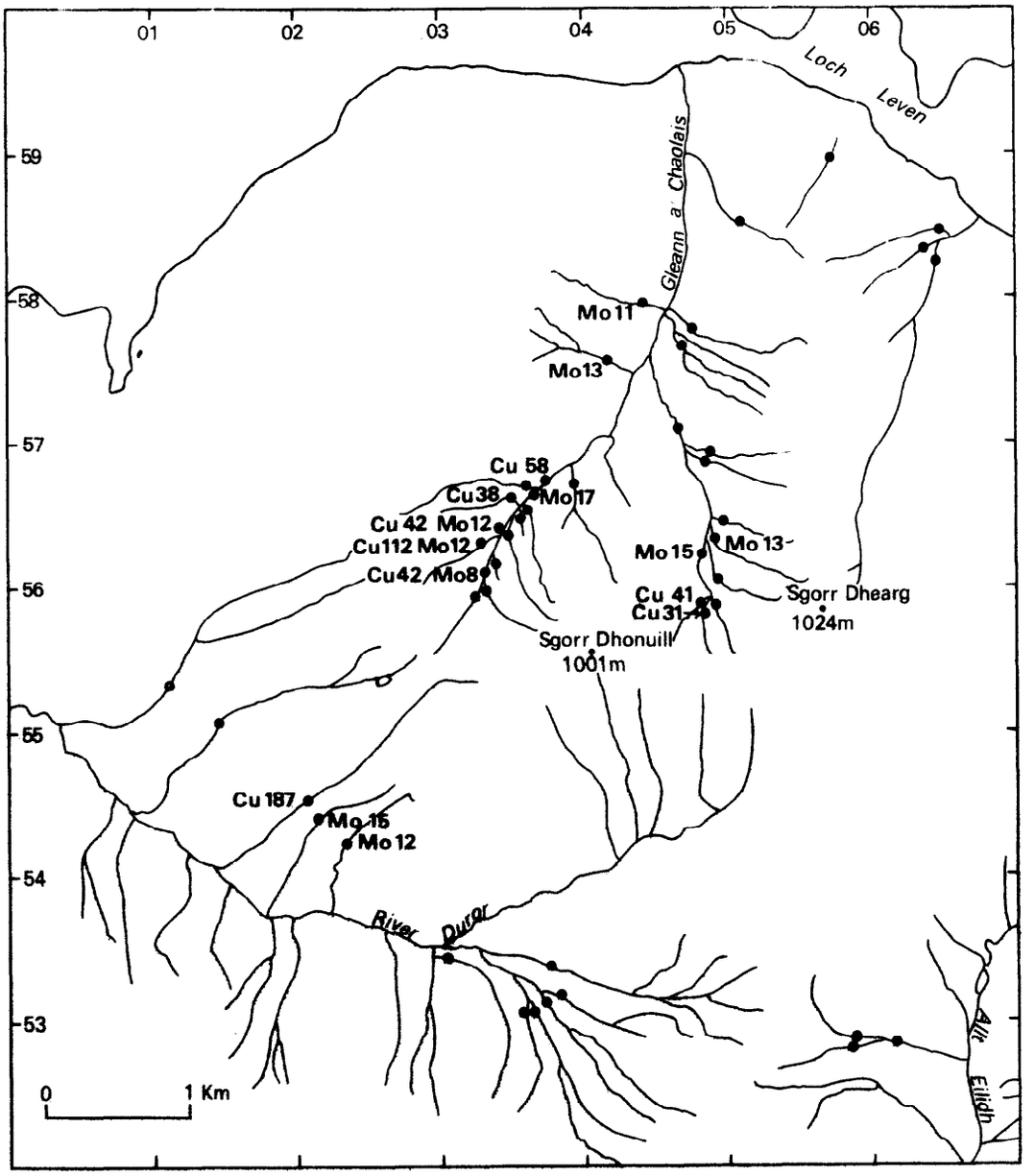

Fig. 12. Panned concentrate sites, showing locations of Cu values ≥ 30 ppm and Mo values ≥ 8 ppm.

Table 2. Chemical analyses and CIPW norms of adamellite samples

	Fresh					Mineralised		Shatter belt		
	XDR 24	XDR 2	XDR 74	XDR 121	Mean	XDR 9	XDR 11	XDR 75	XDR 154	XDR 135
SiO_2	65.62	66.03	66.06	66.18	65.97	67.10	68.68	61.13	66.29	68.64
TiO_2	0.65	0.58	0.56	0.57	0.59	0.40	0.40	1.05	0.53	0.40
Al_2O_3	15.76	15.83	15.78	15.80	15.79	15.49	15.70	16.01	15.89	15.73
Fe_2O_3	1.12	1.55	1.03	1.13	1.21	0.89	0.87	1.79	1.00	1.21
FeO	1.93	1.41	1.57	1.61	1.63	1.45	1.39	2.98	1.64	1.00
MnO	0.05	0.04	0.03	0.04	0.04	0.04	0.01	0.07	0.04	0.03
MgO	1.70	1.67	1.36	1.40	1.53	1.06	1.00	2.95	1.38	0.33
CaO	2.25	2.25	2.30	2.25	2.26	1.88	1.67	2.44	1.71	1.86
Na_2O	4.70	4.70	4.60	4.80	4.70	4.90	4.70	4.60	4.80	5.20
K_2O	4.10	4.20	4.20	4.20	4.18	4.20	4.20	4.60	4.60	3.30
LoI	1.01	1.33	0.73	0.78	0.96	1.68	1.19	2.25	2.04	2.41
H_2O-		0.21	0.07	0.09	0.12	0.14	0.23	0.21	0.10	0.13
P_2O_5	0.22	0.20	0.19	0.18	0.20	0.14	0.14	0.34	0.19	0.14
Total	99.11	100.00	98.48	99.03	99.18	99.37	100.18	100.42	100.21	100.38
Norms										
Q	15.13	15.74	16.34	15.46	15.66	16.84	20.08	7.13	14.97	21.60
Or	24.22	24.81	24.81	24.81	24.66	24.81	24.18	27.18	27.18	19.50
Ab	39.75	39.75	38.90	40.60	39.75	41.44	39.75	38.90	40.60	43.98
An	9.72	9.70	10.01	9.17	9.67	7.88	7.37	9.46	7.24	8.31
C	0.03	0.00	0.00	0.00	0.00	0.00	0.72	0.00	0.36	0.56
Di	0.00	0.12	0.12	0.66	0.21	0.43	0.00	0.34	0.00	0.00
en	0.00	0.05	0.04	0.24	0.08	0.14	0.00	0.12	0.00	0.00
fs	0.00	0.01	0.02	0.08	0.02	0.07	0.00	0.04	0.00	0.00
wo	0.00	0.06	0.06	0.34	0.11	0.22	0.00	0.18	0.00	0.00
Hy	5.87	4.53	4.49	4.33	4.82	3.77	3.68	9.57	4.82	1.05
en	4.23	4.11	3.34	3.25	3.74	2.50	2.49	7.22	3.44	0.82
fs	1.64	0.42	1.15	1.08	1.08	1.27	1.19	2.35	1.38	0.23
Mt	1.62	2.25	1.49	1.64	1.75	1.29	1.26	2.60	1.45	1.75
Il	1.23	1.10	1.06	1.08	1.12	0.76	0.76	1.99	1.01	0.76
Ap	0.52	0.47	0.45	0.43	0.47	0.33	0.33	0.81	0.45	0.33
Trace elements (ppm)										
Li	36	28	28	25	29	18	18	23	18	7
F	510	600	560	650	580	390	440	920	460	480
Cu	10	7	9	8	8	113	24	26	9	5
Zn	49	44	41	43	44	33	7	66	31	29
Rb	139	146	148	151	146	134	131	178	164	134
Sr	1124	1060	1153	1025	1090	850	387	1148	816	353
Y	25	21	20	23	22	16	10	29	19	19
Mo	<2	<2	<2	<2	<2	8	<2	3	<2	<2
Ag	<2	<2	<2	<2	<2	<2	<2	<2	<2	<2
Ba	1301	1323	1339	1237	1300	1315	1327	1355	1480	754
Ce	97	88	68	85	84	66	36	118	69	52
W	<3	<3	<3	<3	<3	32	9	3	5	4
Pb	40	32	37	37	36	25	23	41	28	29
Th	35	34	34	41	36	31	25	43	32	27

Table 3. Chemical analyses and CIPW norms of microadamellite samples.

	Unmineralised			Mineralised		
	XDR 206	XDR 55	Mean	XDR 179	XDR 136	XDR 180
SiO_2	73.10	73.52	73.31	71.03	72.46	72.50
TiO_2	0.15	0.14	0.14	0.15	0.14	0.14
Al_2O_3	15.30	14.56	14.93	14.85	14.57	14.43
Fe_2O_3	0.79	0.41	0.60	0.49	0.36	1.15
FeO	0.35	0.57	0.46	0.72	0.48	0.48
MnO	0.01	0.01	0.01	0.01	0.01	0.01
MgO	0.26	0.18	0.22	0.19	0.13	0.15
CaO	0.76	0.81	0.78	1.28	1.09	0.79
Na_2O	4.48	4.50	4.49	4.40	4.00	4.20
K_2O	4.50	4.70	4.60	4.40	4.60	4.50
LoI	0.54	0.57	1.56	1.61	1.01	1.46
H_2O-	0.13	0.10	0.12	0.11	0.04	0.04
P_2O_5	0.04	0.04	0.04	0.04	0.04	0.04
Total	100.41	100.11	100.26	99.28	98.93	99.89
Norms						
Q	27.94	27.26	27.65	25.39	29.02	29.06
Or	26.59	27.77	27.18	26.00	27.18	26.59
Ab	37.89	38.06	37.98	37.21	33.83	35.52
An	3.51	3.76	3.64	6.09	5.14	3.66
C	1.78	0.70	1.24	0.62	1.13	1.31
Hy	0.65	0.95	0.68	1.16	0.69	0.37
en	0.65	0.45	0.55	0.47	0.32	0.37
fs	0.00	0.50	0.13	0.69	0.37	0.00
Mt	0.73	0.59	0.87	0.71	0.52	1.17
Hm	0.29	0.00	0.00	0.00	0.00	0.34
Il	0.28	0.27	0.28	0.28	0.27	0.27
Ap	0.09	0.09	0.09	0.09	0.09	0.09
Trace elements (ppm)						
Li	8	12	10	7	5	5
F	150	130	140	110	60	220
Cu	9	7	8	105	24	357
Zn	3	7	5	8	6	7
Rb	117	123	120	135	132	130
Sr	648	492	570	239	504	302
Y	12	12	12	10	9	11
Mo	<2	<2	<2	2	2	3
Ag	<2	<2	<2	2	<2	2
Ba	1882	1478	1680	1210	1487	1126
Ce	32	36	34	48	38	42
W		4	4	5	4	3
Pb	31	33	32	11	22	38
Th	26	26	26	21	19	23

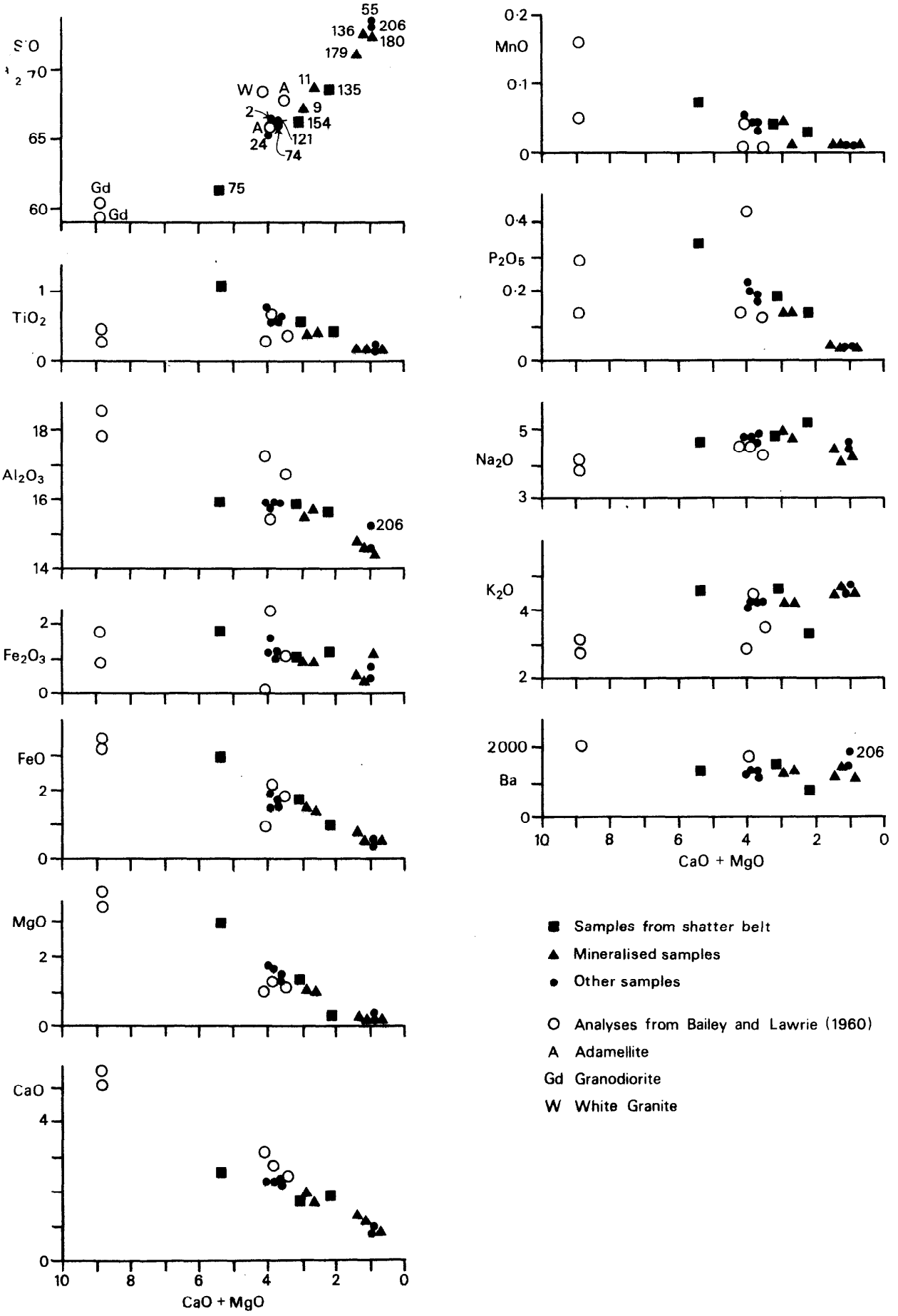

Fig. 13. Variation diagrams for major and minor elements (per cent) and Ba (ppm). For analyses and descriptions of the rocks see Tables 2 and 3.

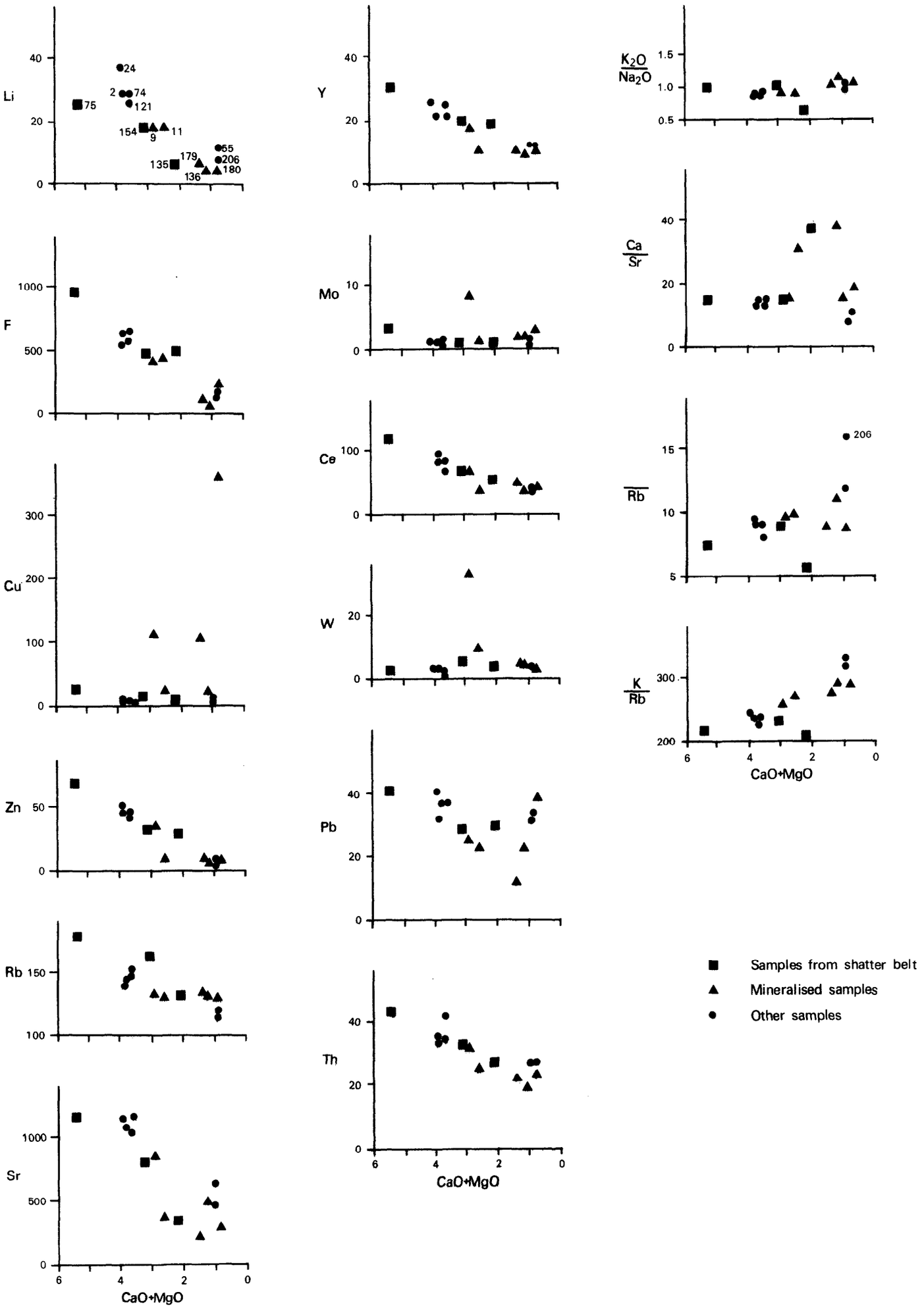

Fig. 14. Variation diagrams for trace elements (ppm).
For analyses and descriptions of the rocks see Tables 2 and 3.

Table 4. Chemical data for five mineralised rock samples

	XDR 267	XDR 268	XDR 269	XDR 271	XDR 272
Ce	40	54	63	25	59
Ba	1167	1115	1508	371	899
Sb	<4	<4	<4	23	<4
Sn	<4	<4	<4	6	<4
Pb	20	43	22	226	33
Zn	4	6	37	17	25
Cu	289	687	185	2289	2102
Ca (%)	0.56	0.52	0.74	0.08	0.40
Ni	<1	1	6	10	8
Fe (%)	0.56	1.03	2.20	1.35	2.01
Mn	100	130	260	180	230
Ti	840	920	2250	1000	2000
Ag	<2	<2	<2	8	2
U	4	6	3	13	11
Rb	136	145	135	110	151
Th	21	18	26	20	28
Nb	11	11	19	<2	19
Sr	286	279	885	142	465
Zr	129	108	233	122	204
Y	11	10	16	6	15
Mo	35	233	68	9257	268
W	50	43	244	491	2434
As	<3	<3	<3	14	37
Bi	<3	<3	<3	6	*
Au	0.022	0.017	<0.01	0.31	0.037

All values in ppm except where otherwise stated
* Not determined.

XDR 267 Microadamellite with disseminated chalcopyrite and rare pyrite. The sulphides also occur on a fracture surface and in a quartz veinlet.

XDR 268 Microadamellite with disseminated chalcopyrite.

XDR 269 Adamellite with disseminated chalcopyrite. Scheelite, molybdenite and chalcopyrite are associated with a quartz veinlet.

XDR 271 Quartz vein containing abundant molybdenite and less chalcopyrite. Country rock is altered adamellite with disseminated chalcopyrite.

XDR 272 Quartz vein with chalcopyrite (altered to goethite, malachite and rare covellite), scheelite and molybdenite. Country rock is altered adamellite with disseminated chalcopyrite.

rather high P_2O_5 values and give evidence of some mobility of Sr (low), Rb (high in two specimens), Ba (low in one and high in another) and K_2O (low in one and high in two).

The overall trends of the trace elements from more basic rocks to acid rocks follow the usual pattern for the Scottish Caledonides (Nockolds and Mitchell, 1948; Nockolds and Allen, 1953; Flett Brown, 1972; Rickard, 1979) except that Rb decreases with decreasing CaO + MgO and BaO does not decrease.

MULTI-ELEMENT ANALYSIS OF FIVE MINERALISED ROCK SAMPLES

Five outcrop samples of mineralised rock were analysed for a wide range of elements (Table 4). Au was determined by neutron activation analysis, the other elements by XRF. The localities from which these five samples were collected are shown in Figure 2. The only ore elements to occur in abundance are Cu, Mo and W. Although slightly enhanced in the mineralised veins (XDR 271 and 272), Sb, Sn, Pb, Ni, Ag, U, As and Bi do not reach concentrations of interest. Au exceeds 0.01 ppm in four of the samples, reaching 0.31 ppm in one of the vein samples.

MULTI-ELEMENT ANALYSIS OF 84 ADAMELLITE AND 26 MICROADAMELLITE SAMPLES

84 outcrop samples of adamellite and 26 of micro-

adamellite (including the 14 samples analysed for major elements but not the five mineralised samples just described) were analysed for selected elements, mostly trace elements, using the methods given above. Sample localities are shown in the geochemical maps, Figures 15–18 and 22, and summary statistics are presented in Tables 5 and 6. For all elements except Cu and Mo the distribution of values is fairly symmetrical and the median and mean provide a clear indication of the central tendency. The microadamellite shows higher median and mean values for Ba and K_2O than the adamellite and lower values for Ce, Pb, Zn, Ca, Mn, Rb, Th, Sr, Y, Li and Na_2O.

Distribution of copper and molybdenum

The geographical distributions of Cu and Mo values are shown in Figures 15–18. Higher values are concentrated in and near the eastern part of the microadamellite, and also in a smaller area to the north. The frequency distributions are strongly skewed and the medians, means and standard deviations (Tables 5 and 6) have little, if any, meaning. Log probability plots of Cu values for the adamellite show a positive change of slope at 12 ppm Cu and 51% of the population, which is interpreted as the threshold between sulphide-free and sulphide-bearing samples. A similar plot for Cu in microadamellite shows a positive change of slope at 12 ppm Cu and 45% of the population. Summary statistics for Cu in the higher and lower populations are given in Table 7. In both rock types the lower populations are nearly symmetrical, both having median Cu values of 6 ppm. Both of the higher populations show distributions which approximate to lognormal, with similar medians (about 50) and geometric means (65 and 69). It should be noted that, although the threshold is taken for convenience at 12 ppm, there is a considerable overlap between the sulphide-bearing and sulphide-free populations. A few sulphide-bearing (particularly pyrite-bearing) samples will lie in the lower population and probably a larger number of sulphide-free samples will fall in the upper population.

Log probability plots of Mo values show less well-defined breaks in slope, but thresholds of possible significance may be discerned at 5 ppm (87% of the adamellite population and 70% for the microadamellite) and 10 ppm (93% and 80%).

In the discussion that follows and in Figs. 19, 20 and 21, a distinction is made between "mineralised" and "unmineralised" samples. The "mineralised" population comprises (a) all samples with >12 ppm Cu, (b) three samples with <12 ppm Cu but >5 ppm Mo (8, 18 and 32 ppm) and (c) two samples with <12 ppm Cu and <5 ppm Mo but with visible sulphide.

The Cu and Mo values for the 36 samples from the 250 x 450 m area in which sulphide mineralisation is best developed may be seen in Figures 16 and 18. Cu values range from 3 to 612 ppm, with a median of 42 ppm and a mean of 88 ppm. Mo values range from <2 to 268 ppm, with a median of 2 ppm and a mean of 18 ppm. Because of preferential collection of mineralised material, the means probably slightly overestimate the average grade over the area in question. Nonetheless the average contents in this area are probably over 50 ppm Cu and 10 ppm Mo.

Inter-element correlation

Inter-element correlation coefficients for the 84 adamellite samples are given in Table 8, for both the natural data and the log-transformed data. In the latter, the Ag and Mo results are omitted because of the large number of values reported as zero which are not amenable to log transformation.

Ca and Mn are strongly correlated, representing the basic-to-acid trend. Li and Zn are correlated with these elements, the former probably occurring in the ferromagnesian silicates and the latter in the same minerals and in Fe–Ti oxides. Ce, Th and Y, probably in rare-earth bearing accessory phases, are correlated with each other, and Ce and Y also, less strongly, with Ca, Mn, Li and Zn. Na_2O, Ba and Sr form another group, representing the Na_2O-bearing feldspars, but not correlating strongly with either Ca or K_2O – indeed Na_2O has a low negative correlation with Ca. Sr also correlates with Li, Mn, Zn, Ce, Th and Y, but its correlation coefficient with Ca is only 0.093. K_2O and Rb are strongly correlated, and Th correlates weakly with both these elements. In the raw data, negative correlation coefficients of >0.3 exist between Ca and Na_2O, Ca and K_2O, and Li and K_2O. The highest correlation coefficients for Cu are 0.269 with Mo and 0.250 with Ag. Also in the range 0.25 to 0.40 are the coefficients for Mo and Ag, Mo and Zn, and Ag and Zn, though these may be distorted because of the large number of results below the detection limits. There is no evidence from the correlation coefficients that mineralisation was related to alkali metasomatism. Apart from Cu, and Mo, and their weak association with Zn and Ag, all the element variability seems to be due to magmatic processes, a result of heterogeneity of the magma.

Scatter plots were computer-plotted for Mn (as a basic-acid index, albeit an imperfect one because of mobility during mineralisation) against each of the other variables. Outliers were found to be mineralised and/or associated with the shatter belt. After removal of these outliers, the plots for Ce, Zn, Ca, Th, Sr (see Figure 19), Y and Li (Figure 20) showed steady decrease with decreasing Mn; K/Rb (Figure 20) showed a diffuse rising trend with decreasing Mn; and Ba (Figure 19), Pb, Cu, Ag, Rb, (Figure 21), Mo, Na_2O, K_2O (Figure 21) and K_2O/Na_2O form clusters without clear trends.

Scatter plots of each pair of Cu, Mo, Rb, K_2O and K/Rb, all form clusters with no important trend, except for a positive trend of Rb against K_2O and a negative one of Rb against K/Rb. Ba shows no trend against K_2O or Rb.

Table 5. Summary statistics for 84 samples of adamellite.

	Min.	Max.	Median	Mean	Standard deviation	Geometric mean
Ce	18	118	56	57	16	55
Ba	332	2127	1337	1301	264	1260
Pb	6	121	30	31	13	28
Zn	7	185	36	37	23	33
Cu	<3	2386	11	86	283	19
Ca (%)	0.16	2.97	0.71	0.73	0.41	0.64
Mn	100	810	265	270	91	258
Ag	<2	8	<2			
Rb	67	183	140	140	18	139
Th	14	43	30	30	5	30
Sr	127	1296	900	837	272	768
Y	8	29	15	16	3	15
Mo	<2	118	<2	6	19	<2
Li	6	66	20	20	8	19
Na_2O (%)	1.9	5.5	4.8	4.7	0.5	4.6
K_2O (%)	2.2	5.4	4.2	4.2	0.4	4.1
K_2O/Na_2O	0.42	2.11	0.89	0.91	0.18	0.89
K/Rb	181	295	249	248	22	247

All element concentrations are in ppm except where otherwise stated

Table 6. Summary statistics for 26 samples of microadamellite.

	Min.	Max.	Median	Mean	Standard deviation	Geometric mean
Ce	21	57	36	36	10	34
Ba	796	1882	1405	1419	240	1398
Pb	<6	52	23	24	10	22
Zn	<1	34	6	8	7	6
Cu	3	406	22	69	110	24
Ca (%)	0.18	1.16	0.36	0.42	0.22	0.37
Mn	60	310	110	120	50	113
Ag	<2	2	<2			
Rb	109	163	132	132	11	131
Th	16	32	22	22	4	22
Sr	130	962	440	463	179	431
Y	7	22	10	11	3	10
Mo	<2	268	2	18	54	2.5
Li	5	12	8	8	2	8
Na_2O (%)	3.3	4.6	4.4	4.3	0.3	4.3
K_2O (%)	4.4	5.3	4.7	4.7	0.2	4.7
K_2O/Na_2O	1.00	1.48	1.08	1.11	0.11	1.10
K/Rb	270	350	295	299	19	298

All element concentrations are in ppm except where otherwise stated.

Table 7. Summary statistics for Cu in higher (>12 ppm) and lower (<12 ppm) populations

	n	Min.	Max.	Median	Mean	Geo. mean
Adamellite						
<12 ppm	43	<3	11	6	6.5	
> 12 ppm	41	14	2386	46	169	65
Microadamellite						
<12 ppm	11	3	10	6	6	
>12 ppm	15	16	406	51	116	69

n = number of analyses

All values in ppm

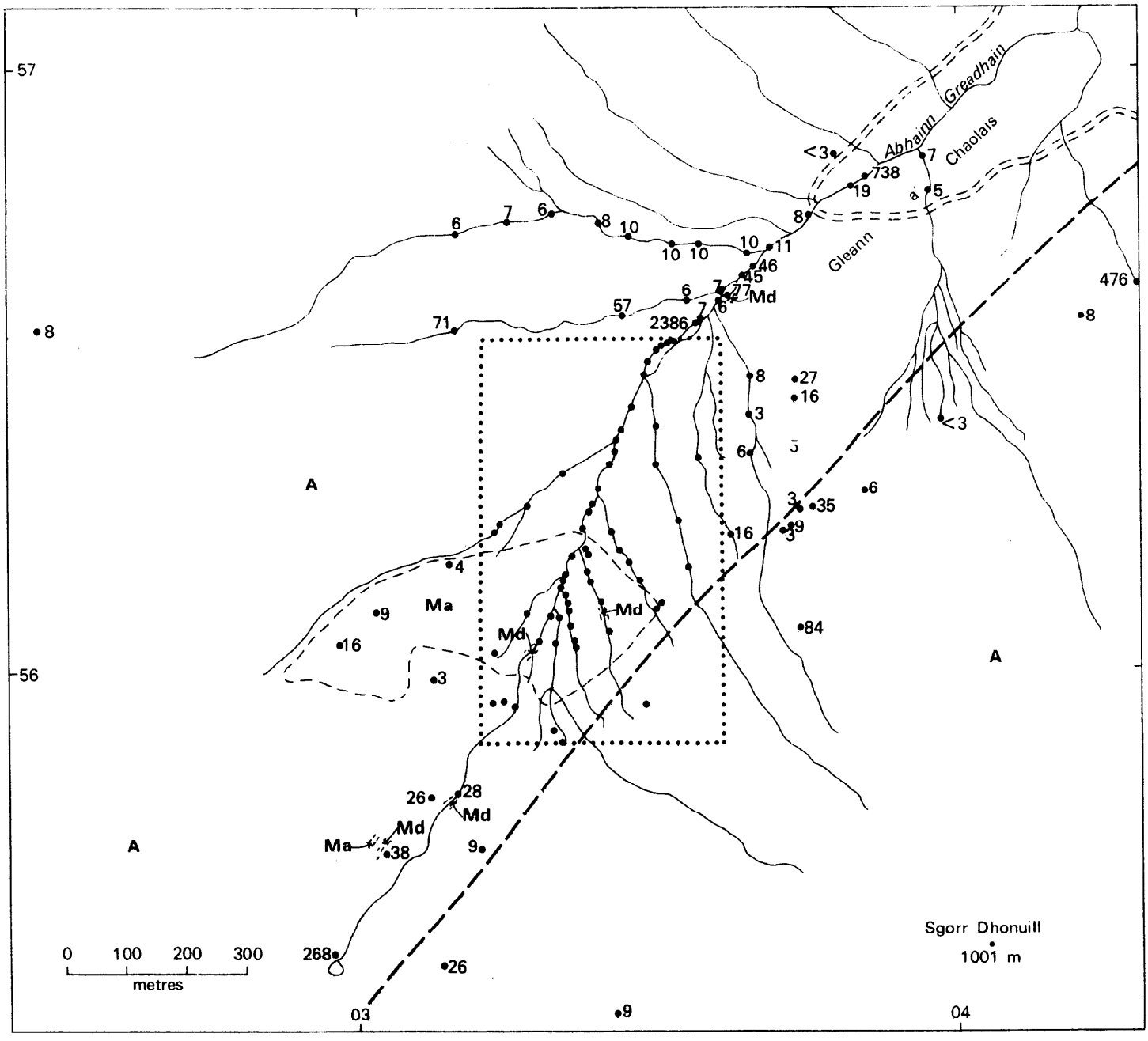

Fig.15 Cu contents of outcrop samples (outer area)

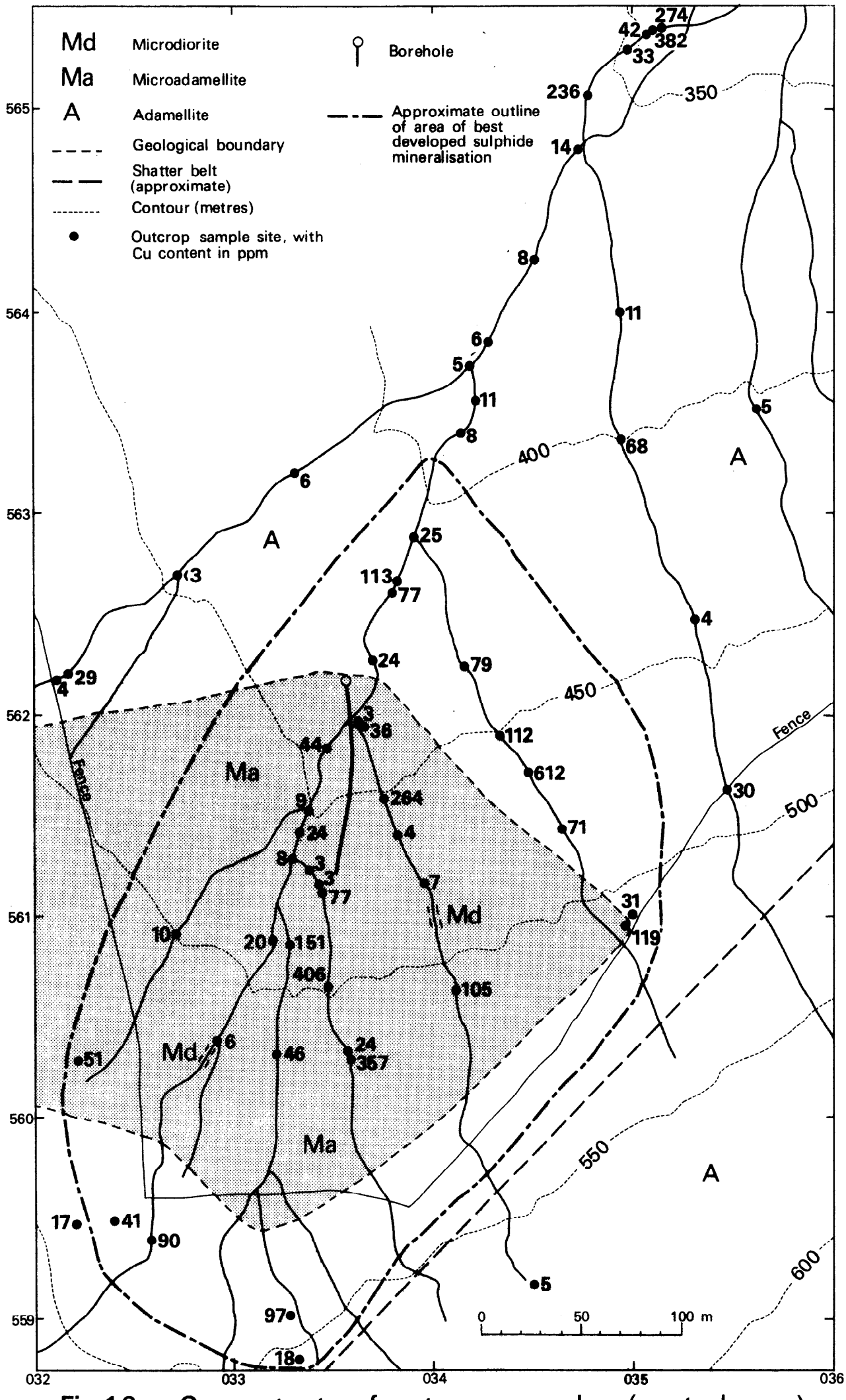

Fig.16. Cu contents of outcrop samples (central area)

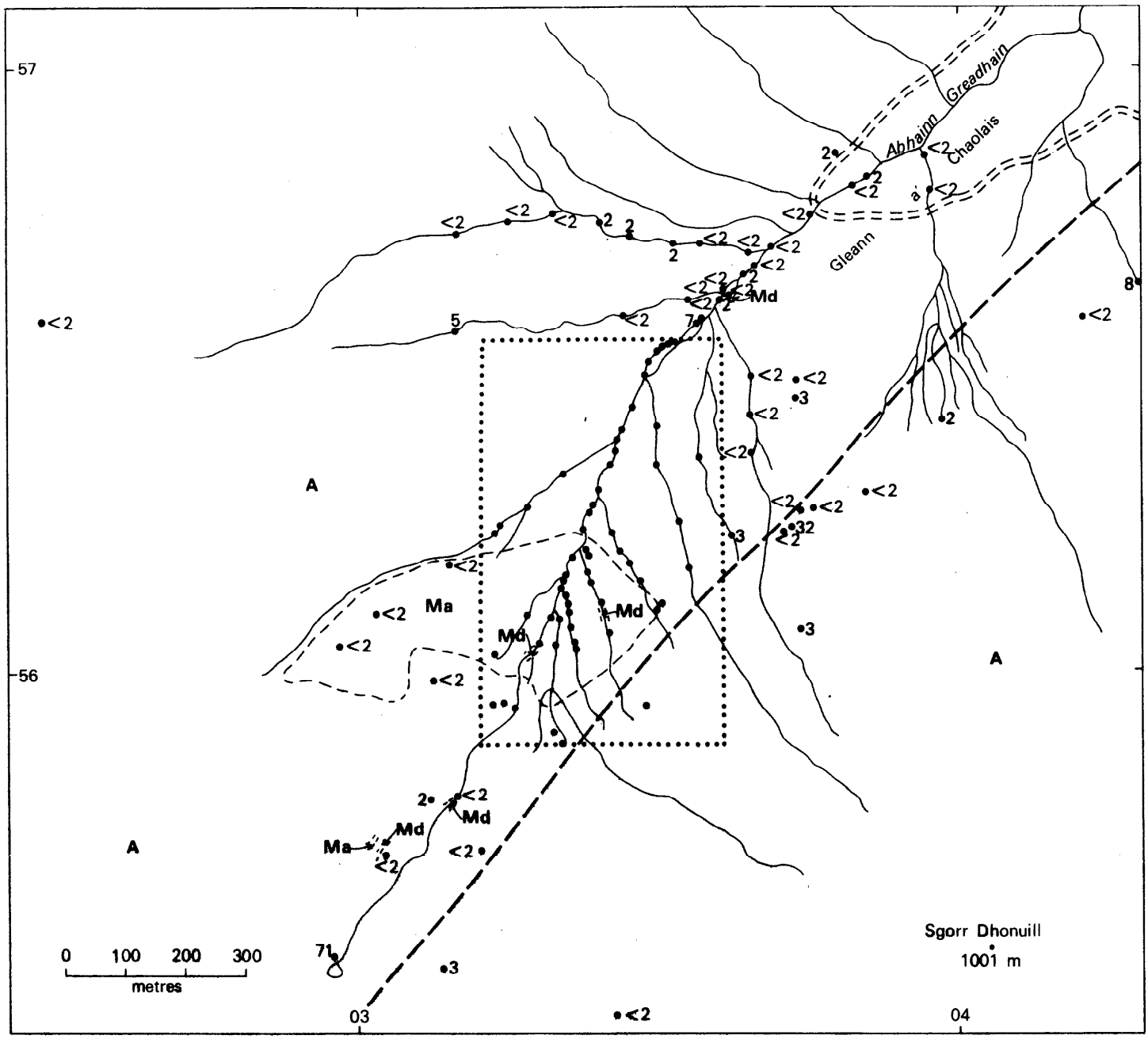

A Adamellite
Ma Microadamellite
Md Microdiorite
==== Forest road
– – – – – Geological boundary
— — — Shatter belt
····· Outline of Figs. 16 and 18
• Outcrop sample site, with Mo content in ppm

Fig. 17 Mo contents of outcrop samples (outer area)

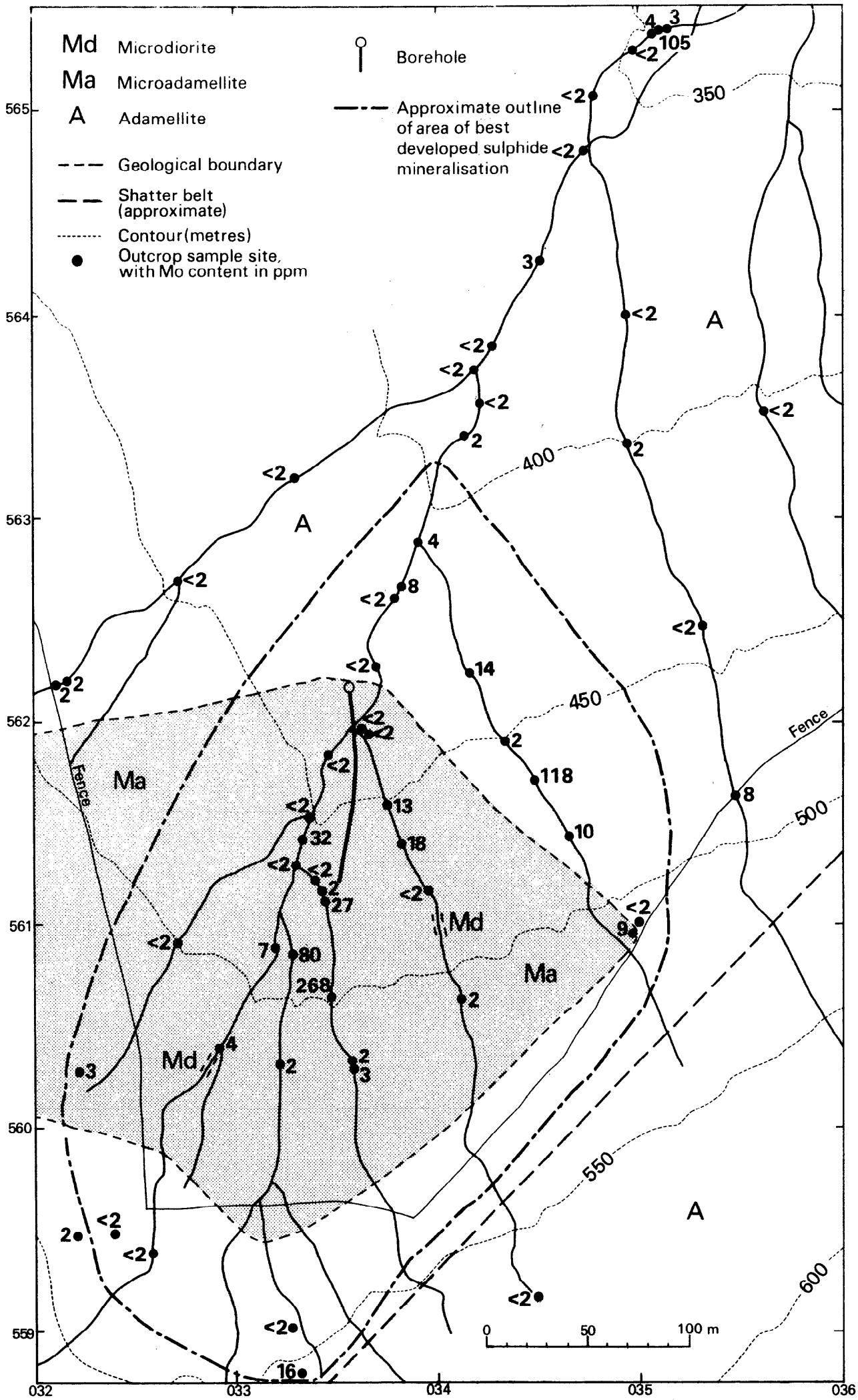

Fig.18. Mo contents of outcrop samples (central area)

Table 8. Inter-element correlation coefficients in 84 samples of adamellite.

	Correlation coefficient				
	0.3–0.4	0.4–0.5	0.5–0.6	0.6–0.7	0.7–0.8
Raw data					
Ce	Zn	Ca, Sr, Li		Mn, Th	Y
Ba	Ag	Na_2O	Sr		
Pb	K_2O				
Zn	Ce, Ag, Y, Mo	Ca	Mn, Li		
Cu					
Ca	Y, $-Na_2O$, $-K_2O$	Ce, Zn	Li		Mn
Mn		Sr, Y	Zn	Ce	Ca, Li
Ag	Ba, Zn, Mo				
Rb	Th, Y				K_2O
Th	Rb	Sr, K_2O	Y	Ce	
Sr	Y	Ce, Mn, Th	Ba, Li, Na_2O		
Y	Zn, Ca, Rb, Sr	Mn	Th		Ce
Mo	Zn, Ag				
Li	$-K_2O$	Ce	Zn, Ca, Sr		Mn
Na_2O	$-Ca$	Ba	Sr		
K_2O	Pb, $-Ca$, $-Li$	Th			Rb
K_2O/Na_2O		$-Ba$, $-Sr$, K_2O	Rb		$-Na_2O$
K/Rb	$-Y$		$-Rb$		
Log-transformed data (omitting Ag and Mo)					
Ce		Sr	Zn, Th, Li	Ca, Mn, Y	
Ba		Pb, Li	Na_2O		Sr
Pb	Th, Y, Na_2O	Ba, Sr, Li			
Zn	Sr		Ce, Y, Li	Ca	Mn
Cu					
Ca			Y, Li	Ce, Zn	Mn
Mn		Sr	Y	Ce, Li	Zn, Ca
Rb	Y	Th			K_2O
Th	Na_2O, Pb	Rb, Sr	Ce, K_2O, Y		
Sr	Zn	Ce, Pb, Mn, Th	Na_2O	Li	Ba
Y	Pb, Rb, Li		Zn, Ca, Mn, Th	Ce	
Li	Y	Ba, Pb	Ce, Zn, Ca	Mn, Sr	
Na_2O	Pb, Th		Sr, Ba		
K_2O			Th		Rb
K_2O/Na_2O	$-Ba$		Rb, $-Sr$, K_2O		$-Na_2O$
K/Rb	$-Zn$, $-Y$, Na_2O		$-Rb$		

Inter-element correlation coefficients for 26 microadamellite samples are given in Table 9, for both natural and log-transformed data. The Ag and Mo results are omitted in the latter, as in the adamellite data.

The elements Ce, Zn, Mn, Th, Sr and Y are positively correlated, representing the frequency of oxide phases and rare-earth-bearing accessory minerals. Ca, representing plagioclase, also correlates with this group, though it is interesting to note that the correlation coefficient between Ca and Sr is only 0.296. Sr correlates additionally with a second group, Ba, Pb and Na_2O, probably representing the soda component of the feldspars. Rb, as expected, correlates closely with K_2O. Li, which in the adamellite correlates with the basic suite of elements and is throught to lie in ferromagnesian silicates, here correlates negatively with Ca and positively, though weakly, with K_2O and Na_2O and is therefore possibly contained in alkali feldspar or white mica. Cu and Mo are more strongly correlated than in the adamellite, and there is a weak negative correlation between Cu and Sr, reflecting Sr loss accompanying mineralisation.

Computer-plotted scatter diagrams of Mn against each of the other variables show no clearly defined trends. The positive correlations with Ce, Zn, Ca, Th, Sr (see Figure 19) and Y are much influenced by two outlying samples (which are not mineralised) and elimination of these points leaves a scatter without trend, except for a slight positive correlation with Ca. There is an indistinct inverse relationship with Rb (see Figure 21).

Scatter plots of each pair of Cu, Mo, Rb, K_2O and K/Rb mostly show no clear trend, but Rb shows a positive trend against K_2O and a negative one against K/Rb. Ba shows a slight negative correlation with Rb.

Geochemistry of Ba, Sr, Li, K and Rb

In Figures 19, 20 and 21 some of the variables which are most likely to be affected by metasomatism accompanying mineralisation or alteration are plotted against Mn. In the adamellite, Mn itself shows high values in three samples from the shatter belt and a number of mineralised samples show low Mn.

Ba (Figure 19) is low in several samples from the shatter belt and one sheared sample from elsewhere, and is high in another sheared sample. Mineralised samples tend to have slightly lower Ba than unmineralised in both adamellite and microadamellite. There is a wider spread of values in the fine rock type than in the coarse, but the central tendencies are similar. Loss of Sr (Figure 19) and Li (Figure 20) commonly accompanies the alteration associated with mineralisation, shearing and the shatter belt. Values of both elements are lower in the microadamellite than in the adamellite.

K_2O and Rb values (Figure 21) in the adamellite tend to be very slightly higher, and more scattered, in samples associated with mineralisation and the shatter belt. In the microadamellite there is a greater spread of K_2O values in the mineralised samples but the central tendency is the same as in unmineralised samples, somewhat higher than in the adamellite; Rb values are lower in the microadamellite than in the adamellite, but there is a slight increase with mineralisation.

The distribution patterns of these five elements thus show evidence of limited compositional change associated with the alteration. Alteration associated with the shatter belt seems to have had rather greater chemical effect than that accompanying the mineralisation. In both, the losses (especially Sr) are more conspicuous than the gains.

The K/Rb ratios are plotted against Mn in Figure 20. It is usual for the K/Rb ratio to decrease on passing from the more basic rocks of an igneous suite to the more acid rocks (e.g. Heier and Billings, 1970). The Ballachulish microadamellite does not conform to this pattern, in that the K/Rb ratios are higher than those of the adamellite and are, moreover, abnormally high for such an acid rock (Tables 5 and 6). If only the fresher, unmineralised samples are considered, the contrast between the rock types is greater: for the adamellite the range of K/Rb values is 210–290 and the median is 252 whereas for the microadamellite the range is 275–350 and the median 308. A possible explanation is that the microadamellite magma was depleted in Rb by the separation of an aqueous fluid with a low K/Rb ratio. This would have taken place in the source magma at depth or, more likely, in situ at the time of emplacement and solidification.

The K/Rb ratios of the mineralised samples are closer, suggesting slight Rb enrichment in the microadamellite accompanying mineralisation. For mineralised adamellite the range is 209–285 and the median 246, and for the microadamellite the range is 270–317 and the median 292. These results may be compared with the trends of K/Rb ratios at other hydrothermal mineral deposits. In Chilean porphyry copper deposits, the hydrothermally altered rocks have lower K/Rb ratios than the parent igneous rocks (Armbrust and others, 1971, 1977; Oyarzun, 1974). This is interpreted as the result of hydrothermal alteration by aqueous fluids which had previously separated from the crystallising magma and which therefore had lower K/Rb ratios than the magma. By contrast, at the Seneca volcanogenic massive sulphide deposit in British Columbia the K/Rb ratios are high, possibly a result of reaction with sea water (Armbrust and Gannicott, 1980). At Ballachulish the mineralising fluids are likely to have been late aqueous separates from the same source as the magmas which formed the adamellite and the microadamellite. (This is supported by the Rb-Sr evidence, see p.38). In contrast to the porphyry and volcanogenic models, the fluids appear not to have introduced much new K or Rb

Table 9. Inter-element correlation coefficients in 26 samples of microadamellite.

	Correlation coefficient					
	0.3–0.4	0.4–0.5	0.5–0.6	0.6–0.7	0.7–0.8	>0.8
Raw data						
Ce	Ca, Ag	Sr	Th, Y	Mn	Zn	
Ba			Sr, Na_2O	Pb		
Pb	–Rb, Na_2O	Sr		Ba		
Zn	Ca			Th	Ce, Sr	Mn, Y
Cu	–Sr			Mo		
Ca	Ce, Zn	Th, Y	–Li	Mn		
Mn				Ce, Ca	Th, Sr	Zn, Y
Ag	Ce					
Rb	–Pb, –Y, $-Na_2O$			K_2O		
Th	K_2O	Ca	Ce	Zn, Sr, Y	Mn	
Sr	–Cu	Ce, Pb, Na_2O	Ba, Y	Th	Zn, Mn	
Y	–Rb	Ca	Ce, Sr	Th		Zn, Mn
Mo				Cu		
Li	Na_2O, K_2O		–Ca			
Na_2O	Pb, –Rb, Li, $-K_2O$	Sr	Ba			
K_2O	Th, Li, $-Na_2O$			Rb		
K_2O/Na_2O	–Sr	–Pb	–Ba, Rb	K_2O		$-Na_2O$
K/Rb	Ba, Pb, Mn, Sr, Y					–Rb
Log-transformed data (omitting Ag and Mo)						
Ce	Pb, Sr	Ca, Th, Y	Mn	Zn		
Ba	–Rb, Li			Na_2O	Pb, Sr	
Pb	Ce, Mn	–Rb	Na_2O	Sr	Ba	
Zn			Th, Sr	Ce, Ca, Y		Mn
Cu	–Th	–Sr				
Ca	Th	Ce, Y, –Li		Zn, Mn		
Mn	Pb, Na_2O		Ce	Ca, Sr	Th, Y	Zn
Rb	–Ba, –Sr, –Y, $-Na_2O$	–Pb		K_2O		
Th	–Cu, Ca, K_2O	Ce, Sr	Zn, Y		Mn	
Sr	Ce, –Rb, Y	–Cu, Th	Zn	Pb, Mn, Na_2O	Ba	
Y	–Rb, Sr	Ce, Ca	Th	Zn	Mn	
Li	Ba, Na_2O	–Ca				
Na_2O	Mn, –Rb, Li, $-K_2O$		Pb	Ba, Sr		
K_2O	Th, $-Na_2O$			Rb		
K_2O/Na_2O		–Sr	–Ba, –Pb, Rb		K_2O	$-Na_2O$
K/Rb	Ba, Pb, –Cu, Mn, Y	Sr				–Rb

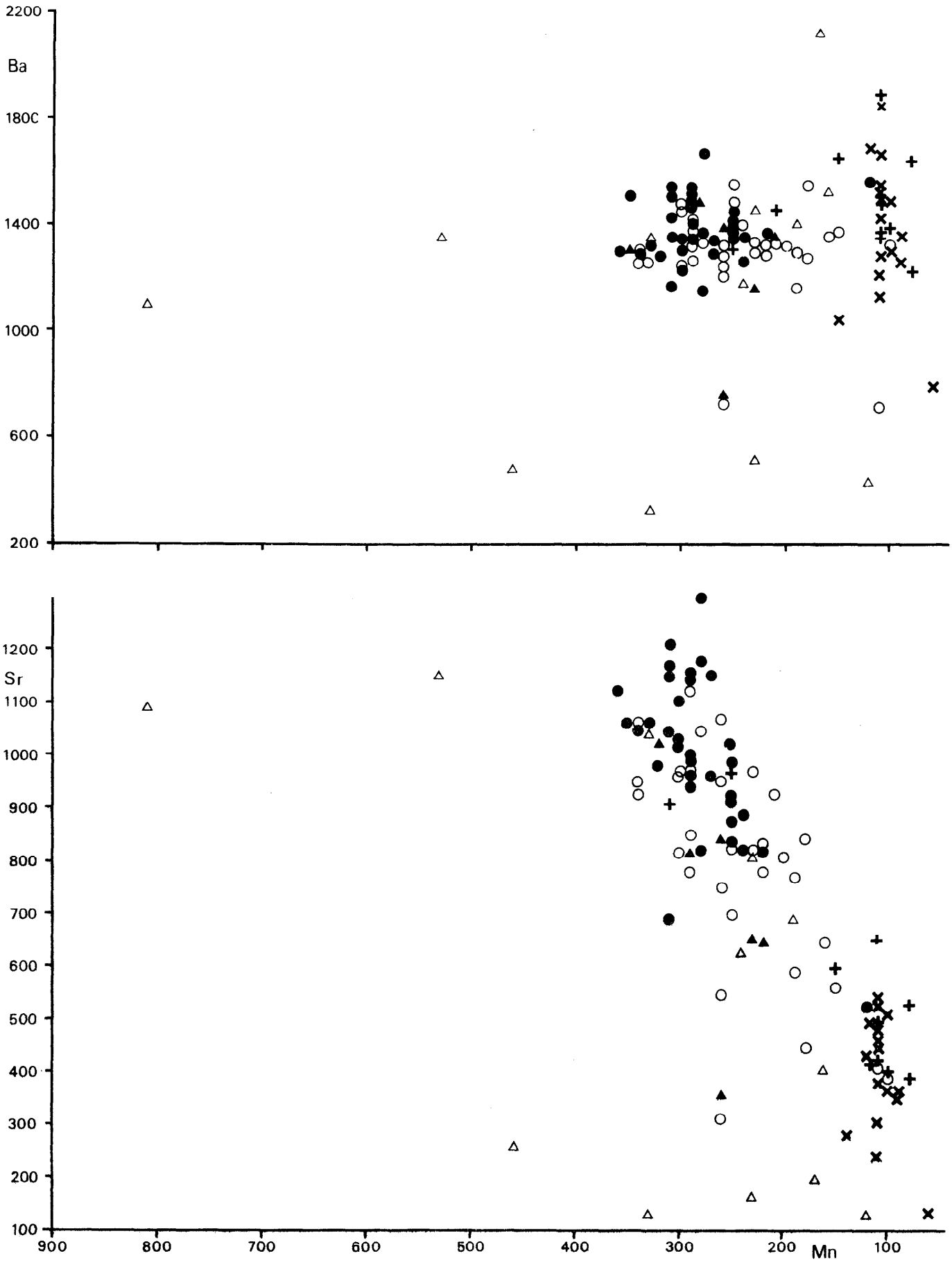

Fig.19. Ba : Mn and Sr : Mn plots for 84 adamellite and 26 microadamellite samples

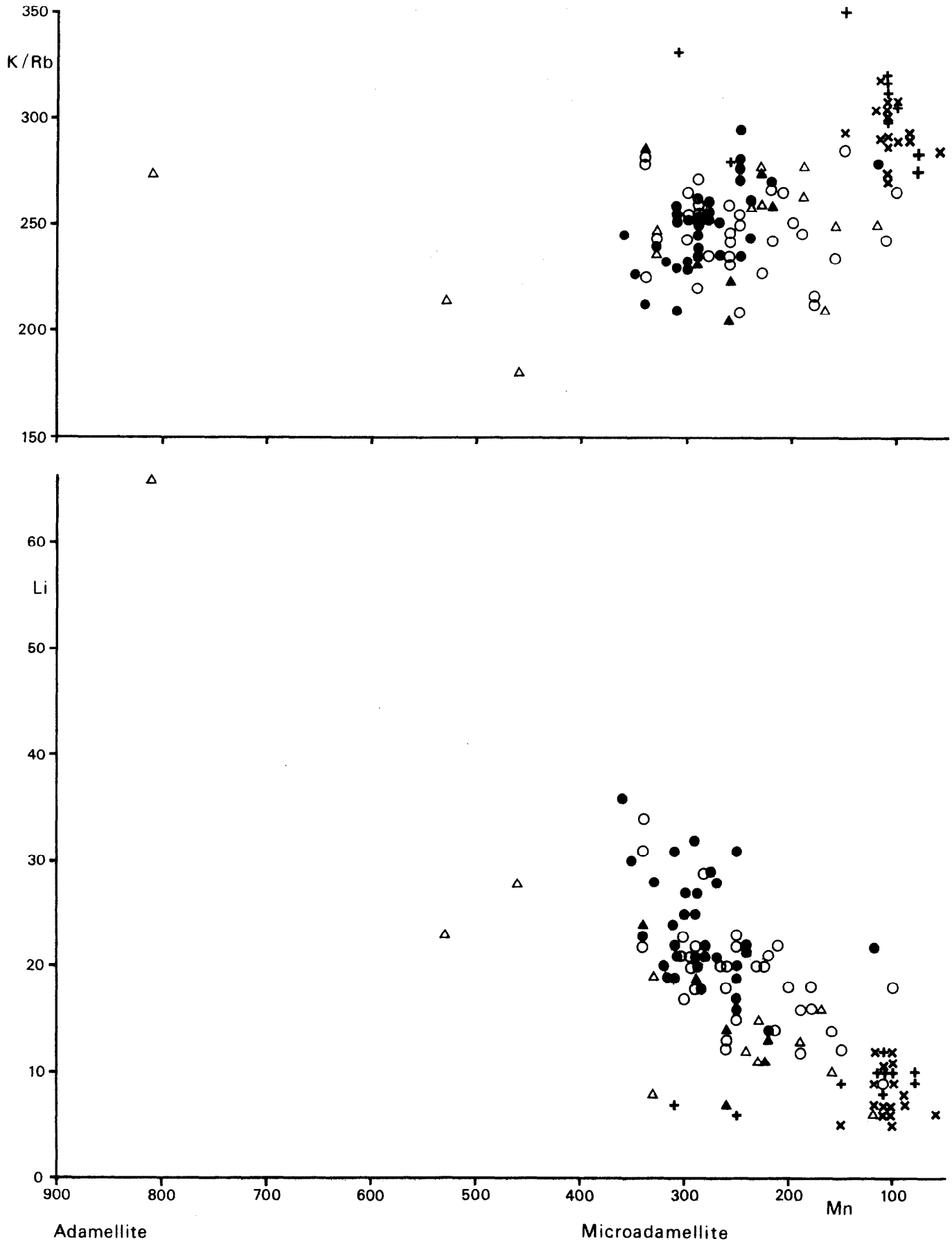

Fig. 20. K/Rb:Mn and Li : Mn plots for 84 adamellite and 26 microadamellite samples

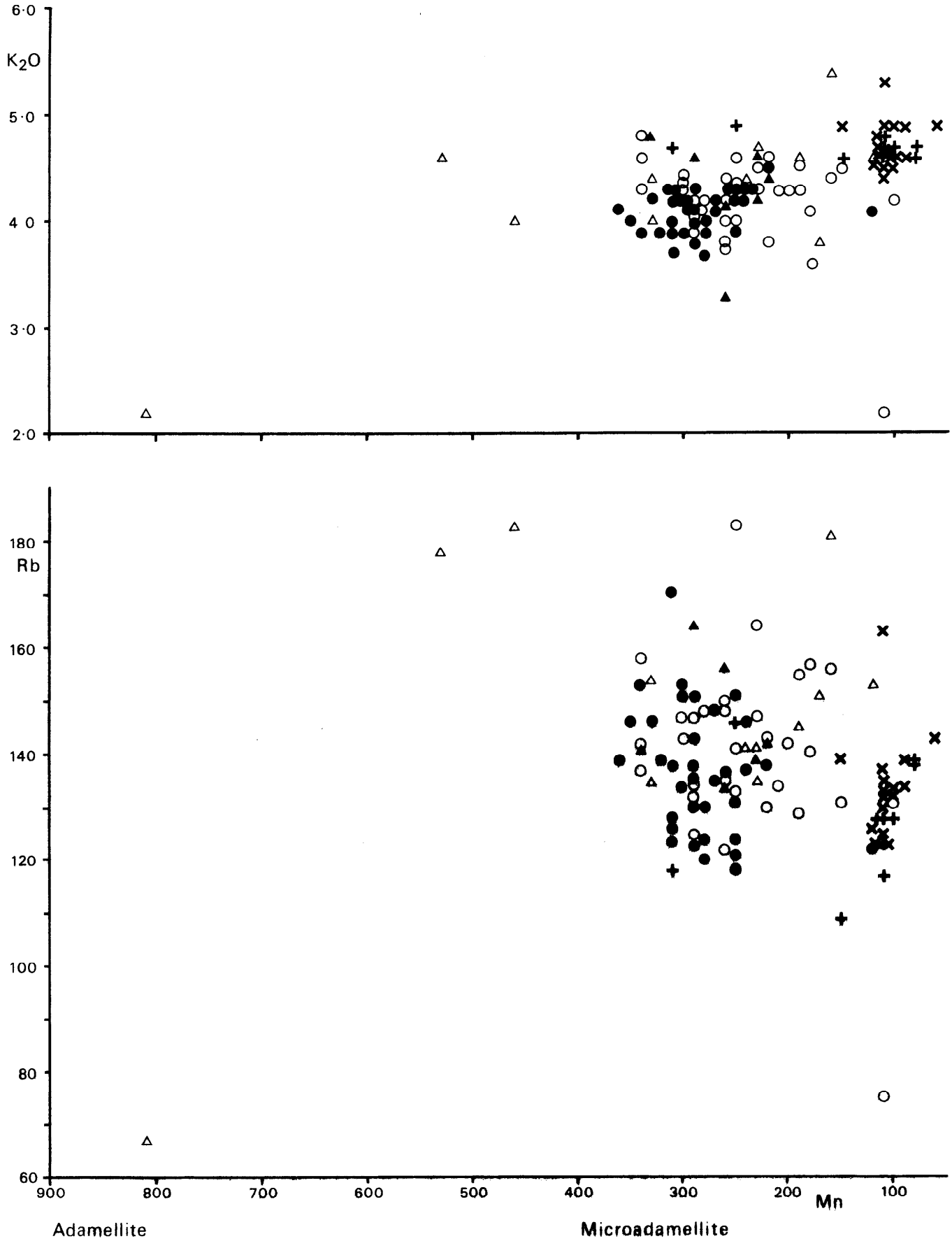

Fig. 21. K_2O: Mn and Rb: Mn plots for 84 adamellite and 26 microadamellite samples

into the system; the values of the K/Rb ratio were little changed in the adamellite while in the microadamellite they were lowered, though only slightly, tending towards the range of values in the adamellite.

The K_2O geochemistry also contrasts with that described at porphyry copper deposits in the small amount of potash metasomatism. Armbrust and others (1977) suggest that sericitic alteration associated with porphyry copper deposits commonly involves an increase in K, though they point out that in the potassic zone K need not be added if the rocks are already sufficiently rich in K. These authors then proceed to show that there are considerable increases in K in the alteration zones of the El Teniente, Rio Blanco and Los Bronces porphyry copper deposits. In the UK, Allen and others (1976) show that there has been K metasomatism in the mineralised rocks at Coed-y-Brenin. At Ballachulish this pattern is not evident.

TUNGSTEN

Tungsten was determined in 38 outcrop samples from the Gleann a' Chaolais area. 33 of these results are shown in Figure 22; locations and W values for the other five are in Figure 2 and Table 4. High W values are associated with high Mo rather than with high Cu. W generally exceeds Mo in mineralised adamellite, but the reverse holds in the microadamellite. In the microadamellite, 8 outcrop samples contained Mo >10 ppm and/or W >15 ppm. Mo values were in the range 13–268 ppm, W<3–56 ppm and W/Mo <0.11–1.43; if only the middle six W/Mo values are taken, the range reduces to 0.2 – 0.6. By contrast, in the 12 adamellite outcrop samples containing Mo >10 ppm and/or W >15 ppm, Mo values were in the range <2–9257 ppm, W 14–2438 ppm and W/Mo 0.1 to 17 or more; the middle eight W/Mo values are in the range 2–9.

GOLD

In addition to those shown in Table 4, three mineralised outcrop samples were analysed for Au. The results, together with those for Cu, Mo, W and Ag, in ppm, area:-

		Au	Cu	Mo	W	Ag
XDR	180	0.058	337	3	3	2
XDR	181	0.162	407	268	56	0
XDR	190	0.041	612	118	376	2

XDR 180 and 181 are microadamellite, XDR 190 adamellite

RARE EARTH ELEMENTS

Rare earth element (REE) concentrations for adamellite XDR 74 and microadamellite XDR 206 are shown in Table 10. The chondrite-normalised REE patterns (Figure 23) resemble those of the Strontian and Foyers complexes (Pankhurst, 1979) and contrast with that of Cairngorm (Plant and others, 1980). As at Strontian and Foyers, the more acid rock shows the lower REE values. The actual concentrations of REEs in the Ballachulish rocks seem to be similar to those in rocks of rather more basic compositions at Strontian and Foyers, indicative of higher REE levels in the parental magma or of less effective fractionation. In the features in which the Strontian patterns differ from those for Foyers, the Ballachulish patterns appear to be intermediate: there are very slight negative Eu anomalies and moderate Dy depletion. The patterns for the adamellite and microadamellite are nearly parallel in the region La to Dy, except for increasing depletion of the heavier elements in the microadamellite.

FLUID INCLUSIONS

From a study of more than 30 outcrop samples, Dr. A.M. Evans concluded: 'The principal fluid inclusions are of low to moderate salinity (type I) running 0-13 equiv. wt. per cent of NaCl and homogenising at 100-300°C. Higher temperatures and salinity values tend to be developed in and close to the microadamellite, suggesting that it may have been an important channelway for rising solutions. Gas-rich (type II) inclusions are present in most sections indicating trapping of a boiling fluid. High salinity (type III) inclusions are very rare' (Evans and others, 1980). He pointed out that, although the widespread development of type III inclusions has been regarded as a favourable indicator of possible economic mineralisation (Nash, 1976), there are a number of porphyry deposits which are rich in types I and II but poor or lacking in Type III. The co-existence of type I and type II inclusions with similar homongenisation and salinity values suggested the trapping of a boiling fluid and led to an estimate of the depth at which trapping took place as less than 2 km..

The more altered and mineralised specimens tend to have a higher density of fluid inclusions and their inclusions tend to yield higher salinities and homogenisation temperatures. The fluid inclusions from rocks in or near to the shatter belt show no characteristic features to distinguish them from the other specimens examined.

Table 10. Rare earth element contents (ppm)

		La	Ce	Nd	Sm	Eu	Tb	Dy	Yb
XDR 74	Adamellite	55	132	51	8.4	1.9	0.80	3.3	2.5
XDR 206	Microadamellite	36	83	26	3.3	0.70	0.30	1.4	0.87

Determined by instrumental neutron activation analysis.

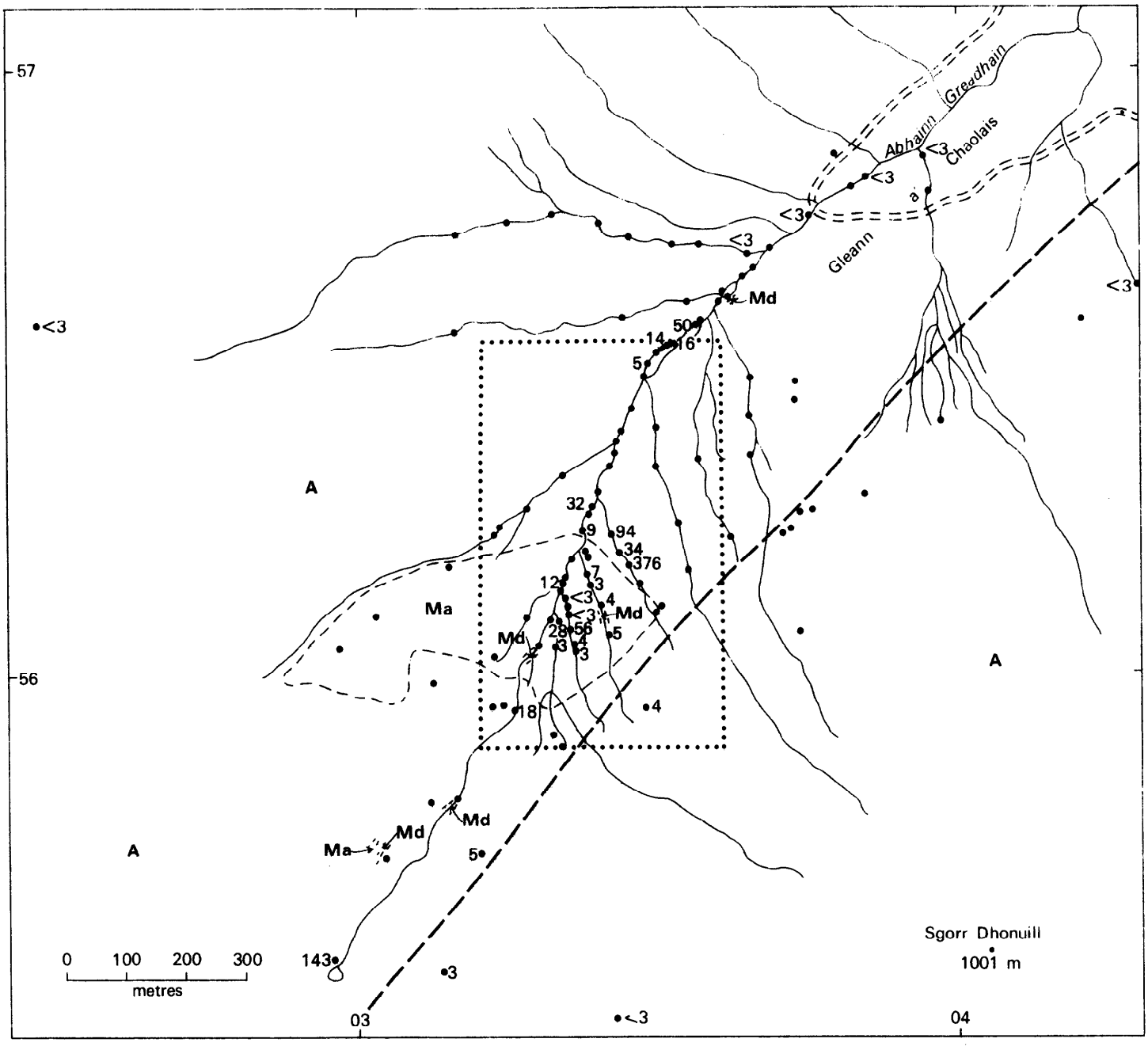

Fig. 22 W contents of outcrop samples

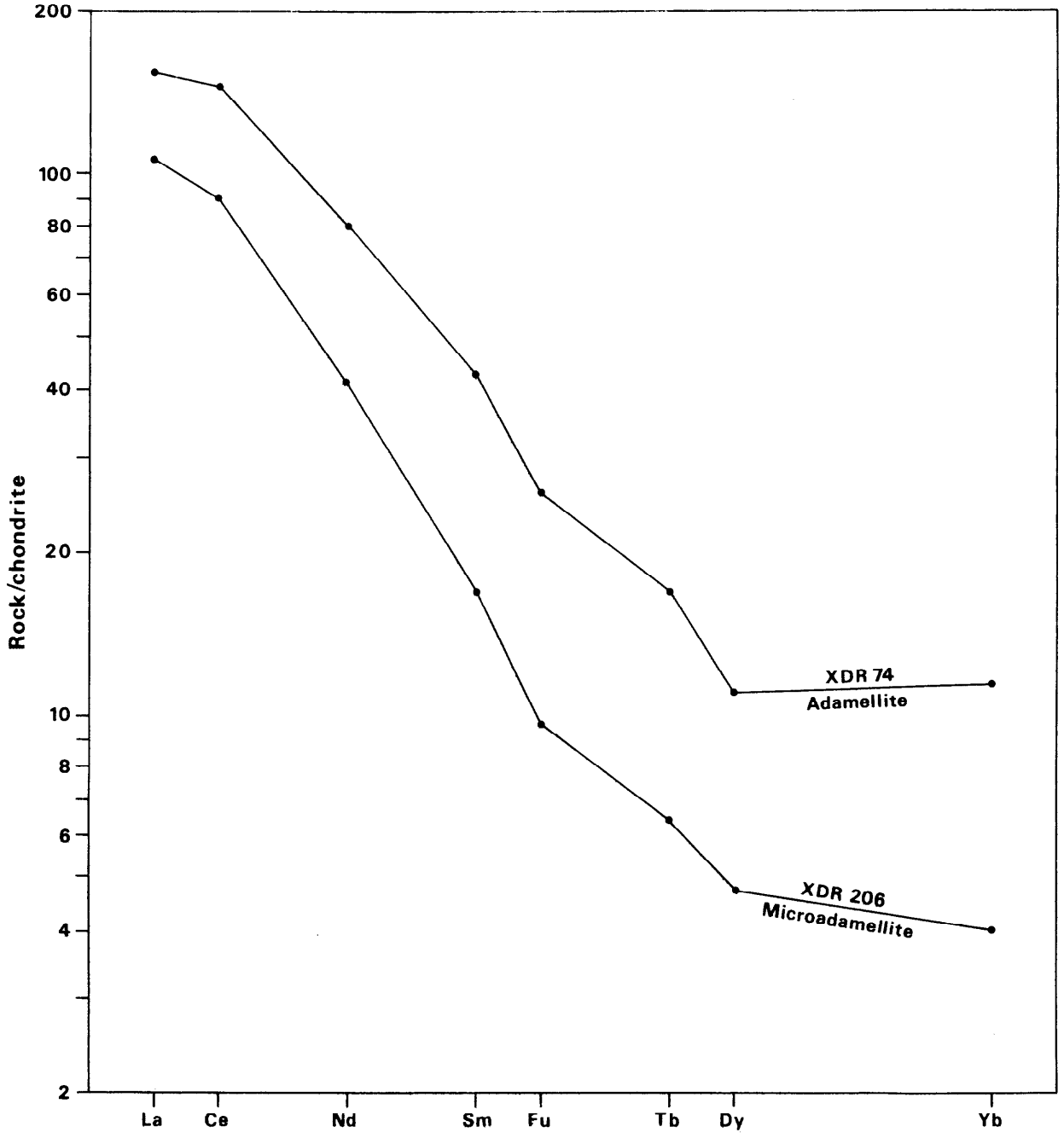

Fig. 23. Chondrite-normalised rare earth element abundances

RB–SR GEOCHRONOLOGY

The Rb-Sr results in this section are from unpublished data supplied by Dr. R.J. Pankhurst and Mrs. M. Brook. Errors are given as ± 2 standard deviations.

Eleven samples of unmineralised adamellite, including three from the present study (XDR 24 and 74 (Figure 2 and Table 2) and XDR 79 from [NN 0245 5657]), gave an isochron representing an age of 406 ± 34 Ma, an initial $^{87}Sr/^{86}Sr$ ratio of 0.70398 ± 0.00020 and MSWD 0.87. Three samples of unmineralised microadamellite (XDR 55 and 206 (Figure 2 and Table 3) and XDR 205 from [NN 0298 5605]), gave a regression line representing an age of 418 ± 77 Ma, initial ratio 0.70419 ± 0.00062 and MSWD 0.66.

Mineralised samples from the adamellite (XDR 9) and microadamellite (XDR 136, 179, 180, 267, 268) fall close to the regression lines for the two host rock types. This suggests that the mineralisation took place a short time after emplacement of the intrusives and that the mineralising fluids did not, to any great extent, modify the $^{87}Sr/^{86}Sr$ ratios of the rocks.

DRILLING

One borehole was drilled, using the Institute's JKS 300 drilling rig, at [NN 0336 5622] (Figs. 16, 18). Total rod length was 578 ft (176.2 m) with a core recovery of 97.75%. The inclination at surface was 59° to the horizontal and the azimuth 180° magnetic. Tropari surveys at 292 ft (89 m) and 573 ft (175 m) gave, respectively, inclination 56° with azimuth 189° magnetic, and inclination 56° with azimuth 193.5° magnetic. The borehole site was at an altitude of about 435 m, and the hole therefore terminated at an altitude of about 280 m.

BQ bits were used to 100 ft (30.5 m) and AQ bits thereafter. The quartz-rich composition and fine grain size made the microadamellite very difficult to drill. Soft-matrix impregnated bits were found to be the most effective, but performance varied substantially between one bit and another and with most bits it remained unsatisfactory. Because of the terrain and the difficulty of constructing an access track, the use of a helicopter was found to be the simplest and most economical way of transporting the plant and equipment to and from the site.

The purpose of the drilling was to find out whether the grade of the mineralisation seen at outcrop increased with depth. The hole was sited to pass under the exposed area of best developed sulphide mineralisation. In order to reach the greatest possible depth, the hole was sited at as low an altitude as possible and a rod-length of 300 m was originally proposed. An inclination of about 60° was selected in order to obtain moderate horizontal cover combined with minimal loss of vertical cover (13% less than a vertical drillhole of the same length). The inclination and azimuth were also such as to enable the borehole to intersect at a high angle the prominent suite of northerly dipping quartz veinlets. In the event, the hole was stopped at 176.2 m because of the difficulty of obtaining suitable bits for the very hard rock and because of the continuing low grade of the mineralisation.

The borehole passed through microadamellite for the whole of its length, except for an intersection with a microdiorite dyke at 112.2–113.4 m. There are minor variations in texture, between the more usual equigranular texture and a microporphyritic tecture in which feldspar crystals of the same size as occur in the equigranular rocks are enclosed in a fine-grained quartzofeldspathic groundmass. There is also some variation in the amount of mafic material (biotite and chlorite) in the core. In the more leucocratic sections there is little or no biotite or chlorite present. The approximate distributions of the more and less leucocratic varieties are given in the borehole log, Appendix I.

GEOCHEMICAL RESULTS

Drilling sludges were collected for XRF analysis representing 10 ft (3 m) lengths of drilling. Selected 10 ft lengths of core were split and were also analysed by XRF. Summary statistics of the analyses are shown in Table 11. The median values for the core samples agree quite closely with those for outcrop samples (Table 6), except for Cu and Mo, which are higher in the core, as would be expected, and Ca, which is also higher in the core but for which there is no obvious explanation other than local compositional variation within the microadamellite. Cu and Mo results, and Au results for a few samples, are plotted on Figure 24, together with chargeability and resistivity logs.

Compared with the core samples, the sludge samples show high values for Zn, Cu, Ni, Fe, Mo and W. This is likely to be due to contamination, since impregnated bits have been found to contain major Fe, Cu, Zn, and Ni, and reamers contain W (R.C. Leake, personal communication). In the top 30 m a Mo-bearing grease was used on the drilling rods, and the Mo contents of the sludges may have been affected by this. There are no exceptionally high Cu, Mo or W values in sludge samples from depths at which the core was not analysed, so it is unlikely that there are any high levels of these elements in these sections of the core.

Correlation between Cu and Mo values in the core analyses and the mineralogy of the core (Appendix I) is moderately good, with a greater abundance of chalcopyrite and molybdenite generally observed in the sections of core richer in Cu and Mo. The maximum Cu and Mo values in core are 264 ppm Cu and 501 ppm Mo, but the average grade is probably in the ranges 50-100 ppm Cu and 20-30

Table 11. Summary statistics for 57 sludge samples and 25 core samples.

	Sludge samples			Core samples		
	Min.	Max.	Median	Min.	Max.	Median
Ce	23	63	39	23	58	34
Ba	860	3404	1465	1010	2779	1496
Sb	<4	6	<4	<4	6	<4
Sn	<4	24	<4	<4	4	<4
Pb	15	72	28	5	24	17
Zn	18	234	94	<3	19	11
Cu	26	499	186	6	264	76
Ca (%)	0.14	1.31	0.70	0.33	1.36	0.93
Ni	3	117	26	<1	5	2
Fe (%)	1.29	15.97	3.55	0.78	1.71	1.14
Mu	60	1620	260	80	190	140
Ti	890	2360	1330	1010	1580	1280
Ag	<2	3	<2	<2	<2	
U	4	19	10	3	12	8
Rb	93	171	128	121	152	136
Th	15	33	21	17	25	22
Nb	8	18	12	10	16	12
Sr	263	640	435	310	647	438
Zr	123	271	176	109	203	156
Y	7	15	9	6	14	10
Mo	5	493	73	<2	501	18
As	<3	21	4	<3	4	<3
W	6	80	19	<3	19	3
Bi	<3	<3		<3	<3	

All values in ppm except where otherwise stated.

ppm Mo. The means for the 25 samples (which include the more mineralised sections of the core) are 95 ppm Cu and 43 ppm Mo.

GEOPHYSICAL LOGGING

The borehole was logged under the supervision of Dr. D. Patrick. Apparent resistivity and chargeability measurements were made using a lateral sonde configuration with a pair of non-polarising potential electrodes 0.1 m apart and centred 1 m below the down-hole current electrode. To reduce inductive coupling influences, a longer receiver delay time was used than in the original survey and the voltage decay curve was integrated between 480 and 1380 millisecs after switch-off.

In the geophysical log (Figure 24), higher chargeabilities and lower apparent resistivities indicate mineralisation between the first measurements below the casing (32 m) and 47 m. This section of core contains sulphides but the Cu content is not very high. A second zone in which mineralisation is indicated by the geophysical results occurs between 68 and 75 m, where the core shows some disseminated pyrite but is not markedly mineralised. There are no major anomalies below this zone and chargeabilities generally lie close to a background level of about 15 ms. Possible small scale mineralisation is indicated at 84, 100, 108 and 143 m and there is some disseminated pyrite and minor chalcopyrite in these sections of core, though not noticeably more than elsewhere. No mineralisation is detected by the geophysics below 145 m, although this is one of the most strongly mineralised sections of the core. This poor agreement between the evidence of the core and the evidence of the geophysical log may be due to the narrow cross-section of the rock sampled by the core and the wider cross-section of rock (diameter c.1 m) to which the geophysical results relate.

CONCLUSIONS

Disseminated Cu-Mo mineralisation occurs in the central part of the Ballachulish igneous complex. The host rocks are the last two members of the plutonic suite, the adamellite and microadamellite. The microadamellite is a small (650 m x 250 m) body emplaced within the adamellite, probably before the latter had completely solidified. Its fine grain size is indicative of rapid cooling and its anomalously low Rb content may be attributed to the separation of a quantity of Rb-enriched aqueous fluid from the microadamellite magma at or before the time of emplacement. After a short interval, this fluid, or derivatives of it, became mobile within parts of the solidified adamellite and microadamellite, resulting in phyllic alteration of the host rocks and the deposition of ore minerals (chalcopyrite, pyrite and molybdenite, with minor

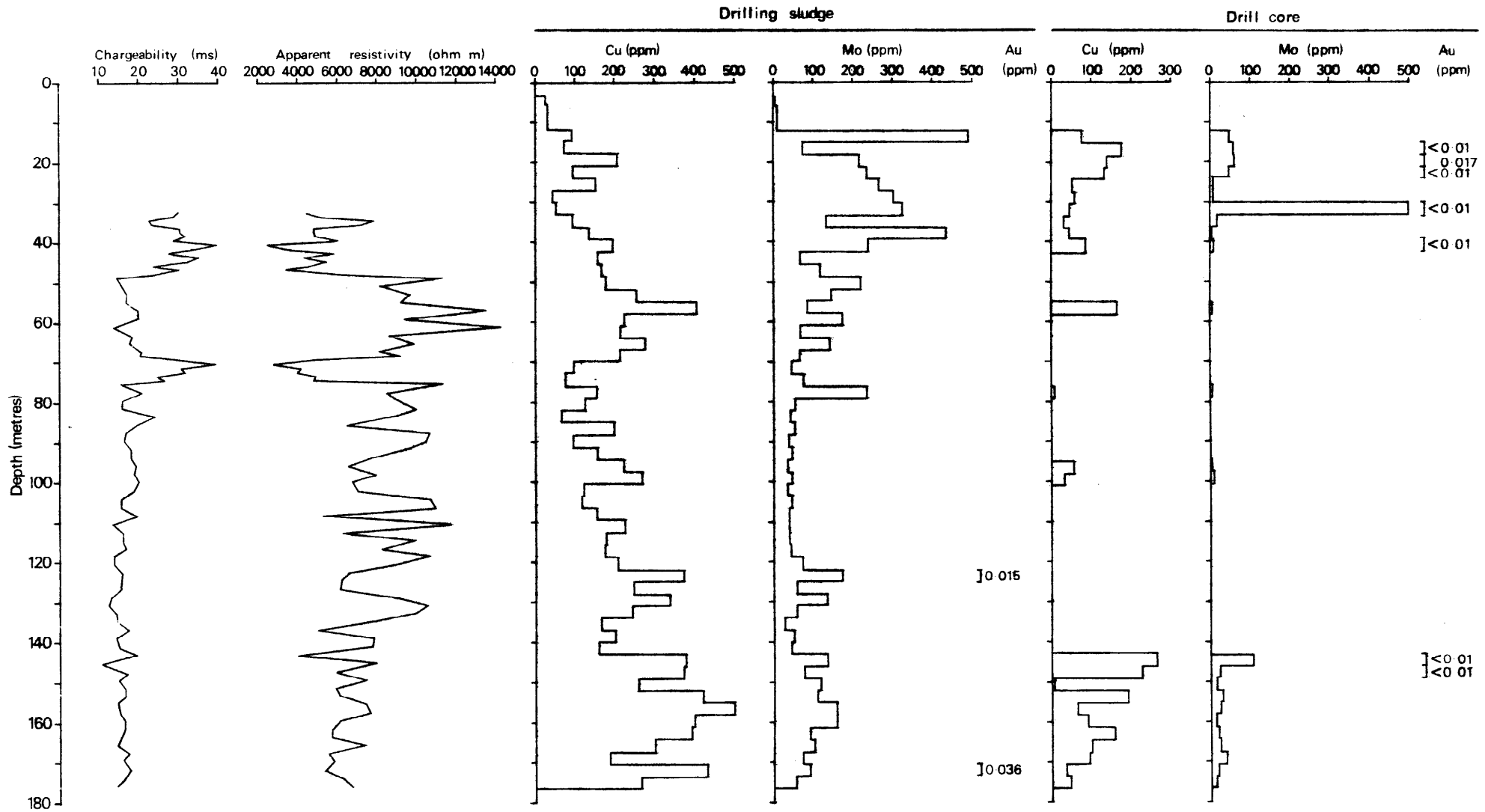

Fig. 24. Geophysical logs and Cu, Mo and Au data for borehole

schcelite and bornite) in fractures and as disseminations. Fluid inclusion studies (Evans and others, 1980) showed that the mineralising fluids were of low to moderate salinity and suggested the trapping of a boiling fluid at a depth of less than 2 km. The main structural control of the mineralisation appears to be the microadamellite. A NNE trending shatter belt outcrops to the southeast of the microadamellite and the main mineralisation. There is no evidence as to whether this fault acted as a control at depth for the mineralisation, nor as to whether, as a result of displacement along the fault, the microadamellite and/or the mineralisation might exist at depth to the southeast of the belt.

The mineralisation thus has several similarities with the classic porphyry copper model (e.g. Lowell and Guilbert, 1970), but it differs in its small scale and weak intensity. Thus (1) the grade of mineralisation is low, (2) although there is well-developed and intense phyllic alteration, there is no potassic alteration zone exposed and the peripheral propylitic alteration is sporadic, (3) the fluids were of lower salinity than those most characteristically associated with porphyry copper deposits, and (4) there was very little K or Rb metasomatism associated with the mineralisation and alteration.

The Ballachulish mineralisation thus offers a model for a low-intensity hydrothermal mineralising system, which may be distinguished from the established models for porphyry mineralisation. It should be noted that it is not only in the core of the hydrothermal system that the models differ but also in the outer zones, where, in the classic porphyry model, well-defined alteration zones (Lowell and Guilbert, 1970) and enhanced K/Rb ratios (Armbrust and others, 1977) are characteristic. It may be suggested that the recognition, in an area of disseminated Cu-Mo mineralisation, of the features listed above should be regarded as an indication that the mineralisation is likely to be of sub-economic grade.

The present study establishes the existence of disseminated copper and molybdenum mineralisation, possibly grading 50-100 ppm Cu and 10-30 ppm Mo with lower values of W, over an area of 250 x 450 m and over a minimum vertical interval, from the highest exposure to the bottom of the borehole, of about 250 m. The results provide no good reason to suppose that mineralisation of economic grade and scale exists, although the model just described may not accurately represent the distribution of mineralisation at any specific locality, and it remains possible that further exploration at depth might penetrate higher metal values.

ACKNOWLEDGEMENTS

The authors are grateful to the Forestry Commission, and in particular to Mr. R. Harvey, Forester in Charge, for access and for cooperation throughout the field investigations. We thank Dr. I.D. Muir for permission to quote from his Ph. D. thesis, and Dr. R.J. Pankhurst and Mrs. M. Brook for permission to use their Rb-Sr data. Messrs. R. Falconer and B. Scarth operated the drilling rig, Mr. K.E. Beer and Dr. W.J. McCourt assisted as site geologist during the drilling, Mr. K Turton carried out the geochemical drainage sampling and Messrs. T.K. Smith, A.E. Davis and D. Peachey were responsible for the chemical analyses.

REFERENCES

ALLEN, P.M., COOPER, D.C., FUGE, R. and **REA, W.J.** 1976. Geochemistry and relationships to mineralization of some igneous rocks from the Harlech Dome, Wales. *Trans. Instn Min. Metall. (Sect. B: Appl. earth sci)*, Vol. 85, pp. B100–B107.

ARMBRUST, G.A. and **GANNICOTT, R.A.** 1980. K/Rb ratios as a source indicator for hydrothermal fluids at the Seneca volcanogenic massive sulphide deposits, British Columbia. *Econ. Geol.*, Vol. 75, pp. 466–477.

— **OYARZUN. J.** and **ARIAS, J.** 1971. Rubidium as a guide to ore at El Teniente (Braden), Chile [abs.] *Econ. Geol.*, Vol. 66, p. 977.

——— 1977. Rubidium as a guide to ore in Chilean porphyry copper deposits. *Econ. Geol.*, Vol. 72, pp. 1086–1100.

BAILEY, E.B. and **LAWRIE, T.R.M.** 1960. The geology of Ben Nevis and Glen Coe and the surrounding country (Explanation of sheet 53). *Mem. Geol. Surv. Scotland.*

BROWN, P.E., MILLER, J.A. and **GRASTY, R.L.** 1968. Isotopic ages of late Caledonian granitic intrusions in the British Isles. *Proc. Yorks. Geol. Soc.*, Vol. 36, pp. 251–276.

EDWARDS, L.S. 1977. A modified pseudosection for resistivity and IP. *Geophys.*, Vol. 42, No.5, pp. 1020–1036.

EVANS, A.M. 1977. Copper-molybdenum mineralization in the Ballachulish granite, Argyllshire, Scotland. *Trans. Instn Min. Metall. (Sect. B: Appl. earth sci.)*, Vol. 86, pp. B152–B153.

— **HASLAM, H.W.** and **SHAW, R.P.** 1980. Porphyry style copper-molybdenum mineralisation in the Ballachulish igneous complex, Argyllshire. *Proc. Geol. Ass.* Vol. 19, pp. 47–51.

FLETT BROWN, J. 1972. *Rb-Sr studies and related geochemistry on the Caledonian calc-alkaline igneous rocks of N.W. Argyllshire.* Ph. D. Thesis, University of Oxford.

FOX, R.C., HOHMANN, G.W., KILLPACK, T.J. and **RIJO, L.** 1980. Topographic effects in resistivity and induced-polarization surveys. *Geophys.*, Vol. 45, No.1, pp. 75–93.

HARMON, R.S. and **HALLIDAY, A.N.** 1980. Oxygen and strontium isotope relationships in the British late Caledonian granites. *Nature*, Vol. 283, pp. 21–25.

HEIER, K.S. and **BILLINGS, G.K.** 1970. In *Handbook of geochemistry* (Wedepohl, K.H., ed.) (Berlin–Heidelberg – New York : Springer), Vol. 11/4, chap. 37.

JOHNSTONE, G.S. 1954. A re-investigation of the Steall area, upper Glen Nevis. *Trans. Ed. Geol. Soc.*, Vol. 16, pp. 167–177.

— 1966. *British regional geology : The Grampian Highlands.* Institute of Geological Sciences.

LITHERLAND, M. 1980. The stratigraphy of the Dalradian rocks around Loch Creran, Argyll. *Scott. J. Geol.*, Vol. 16, pp. 105–123.

LOWELL, J.D. and **GUILBERT, J.M.** 1970. Lateral and vertical alteration-mineralisation zoning in porphyry ore deposits. *Econ. Geol.*, Vol. 65, pp. 373–408.

MILLER, J.A. and **BROWN, P.E.** 1965. Potassium-argon age studies in Scotland. *Geol. Mag.*, Vol. 102. pp. 106–134.

MUIR, I.D. 1950. *Contamination and hybridism in the Ballachulish complex, Argyll.* Pt II of Ph. D. Thesis, University of Cambridge.

NASH, J.T. 1976. Fluid inclusion petrology – data from porphyry copper deposits and application to exploration. *Prof. Pap. U.S. Geol. Surv.*, No. 907–D.

NELSON, P.H. 1977. Induced-polarization effects from grounded structures. *Geophys.*, Vol. 42, No. 6, pp. 1241–1253.

NOCKOLDS, S.R. and **ALLEN, R.** 1953. The geochemistry of some igneous rock series. Part I. *Geochim. Cosmochim. Acta*, Vol. 4, pp. 105–142.

— and **MITCHELL, R.L.** 1948. The geochemistry of some Caledonian plutonic rocks: a study in the relationship between the major and trace elements of igneous rocks and their minerals. *Trans. R. Soc. Edin.*, Vol. 61, pp. 533–575.

OYARZUN, J. 1974. Rubidium and strontium as a guide to copper mineralization emplaced in some Chilean andesite rocks (abs). *5th Int. Geochem. Explor. Symp.*, Vancouver, 1974, p. 333.

PANKHURST, R.J. 1979. Isotope and trace element evidence for the origin and evolution of Caledonian granites in the Scottish Highlands. In *Origin of granite batholiths: geochemical evidence* (Atherton, M.P. and Tarney, J., eds) (Orpington : Shiva Publishing Ltd.), pp. 18–33.

PLANT, J., BROWN, G.C., SIMPSON, P.R. and **SMITH, R.T.** 1980. Signatures of metalliferous granites in the Scottish Caledonides. *Trans. Instn. Min. Metall. (Sect. B : Appl. earth sci.)*, Vol. 89, pp. B198–B210.

READ, H.H. 1961. Aspects of Caledonian magmatism in Britain. *L'pool Manchr. Geol. J.*, Vol. 2, pp. 653–683.

RICKARD, A.J.R. 1979. Petrogenesis of copper-bearing diorites near Kilmelford, West Scotland: geochemical studies (abs). *Trans. Instn Min. Metall (Sect. B: Appl. earth sci.)*, Vol. 88, p. B29.

SIMPSON, P.R., BROWN, G.C., PLANT, J. and **OSTLE, D.** 1979. Uranium mineralisation and granite magmatism in the British Isles. *Phil. Trans. R. Soc. Lond.*, Vol. A291, pp. 385–412.

APPENDIX I BOREHOLE LOG

0 – 1.4	Overburden
1.4 – 176.2	The main rock type is microadamellite, leucocratic (1.4 – 30, 31 – 33, 34 – 48, 67 – 69, 74 – 75, 88 – 112, 137 – 140, 145 – 167) to biotite (or chlorite) bearing (30 – 31, 33 – 34, 48 – 67, 69 – 74, 75 – 88, 113 – 137, 140 – 145, 167 – 176.2). Generally hard, but locally broken. The core is cut by fractures in various directions. Some fracture surfaces are coated with a dark green chlorite, and some by a pale green dioctahedral mica or illite (XRD by D. Atkin). The mineralised fractures and veinlets (containing one or more of quartz, pyrite, chalcopyrite, molybdenite, and, rarely, bornite) are mostly straight-edged and perpendicular to the length of the core (especially the quartz-chalcopyrite veinlets) but the unmineralised fractures, calcite veinlets and a few quartz veinlets are irregular in direction. Some molybdenite and pyrite-bearing fractures are also irregular. Details of these and other features are given below.
3.7	Quartz-chalcopyrite veinlet.
6.4	Disseminated chalcopyrite.
6.7	Quartz veinlet with chalcopyrite.
7.0	Disseminated pyrite.
8.1	Pyrite in and near a quartz veinlet.
8.5	Quartz-pyrite-molybdenite veinlet.
9.1 – 10.1	Sporadic molybdenite.
10.4	Pyrite, disseminated and in a pod.
12.2	Quartz-pyrite veinlet, with molybdenite nearby.
12.6	Quartz-pyrite-molybdenite veinlet.
13.1	Quartz-pyrite veinlet.
13.9	Pyrite-molybdenite veinlet.
14.0	Quartz-chalcopyrite veinlet.
14.5	Molybdenite coating on irregular fracture surface, contrasting with the usual planar mineralised fractures.
14.9	Quartz veinlet with pyrite, chalcopyrite and bornite. Minor covellite associated with bornite is probably an alteration product. Pyrite and chalcopyrite are disseminated nearby.
14.9 – 18.0	Only 0.8 m of core, broken. ? cavity.
15.0	Quartz-chalcopyrite veinlet.
18.6	Molybdenite and pyrite on fracture surface.
18.9 – 19.2	Fine-grained molybdenite on fracture surface.
19.2	Unmineralised quartz veinlet cut and displaced by calcite vein. Chlorite and dioctahedral mica fracture coating.
19.7	Fine-grained molybdenite on fracture.
19.8	Quartz-chalcopyrite veinlet.
20.1	Quartz-chalcopyrite-bornite veinlet.
20.6	Quartz-chalcopyrite veinlet, cut by fracture with fine-grained molybdenite.
20.9	Quartz-chalcopyrite veinlet.
21.3	Quartz veinlet with molybdenite and chalcopyrite. Trace pyrite, chalcopyrite and arsenopyrite disseminated nearby.
21.9	Quartz-chalcopyrite veinlet.
22.6	Quartz-pyrite veinlet.
23.5	Quartz-pyrite-chalcopyrite-molybdenite veinlet.
23.8	Quartz-pyrite veinlet.
23.9	Quartz-chalcopyrite veinlet.
24.4	Pyrite in quartz veinlets and associated dissemination.
25.3	Quartz-chalcopyrite veinlet.
26.3	Quartz veinlet with chalcopyrite, pyrite and minor bornite.
26.5	Quartz-pyrite-chalcopyrite veinlet, 30° to length of core.
26.8	Quartz-chalcopyrite veinlet.
26.9	Quartz-pyrite veinlet cut by shear with chloritic coating and by irregular calcite veinlets.
27.2	Quartz-pyrite veinlet.
27.8	Irregular pool of quartz (outer) and calcite (filling).
28.0	Pyrite veinlet.
28.3	A little disseminated pyrite.
28.7	Fracture surface coated with pyrite.
29.0	Fracture surface coated with pale green dioctahedral mica.
30.9	Chalcopyrite and molybdenite in and near an irregular quartz veinlet trending at 30° to length of core.
31.1	Molybdenite-pyrite fracture coating and irregular quartz-molybdenite veinlet.
31.1 – 31.4	Irregular veinlets of molybdenite.
32.0	Two quartz-chalcopyrite veinlets.
32.3	Quartz-chalcopyrite veinlet and, at an angle, quartz-molybdenite veinlets which are contemporary or later. Fracture coating of pale green dioctahedral mica.
32.6	Quartz-molybdenite veinlet, perpendicular to length of core.
34.4	Quartz-pyrite veinlet.
34.9	Two quartz-chalcopyrite-molybdenite-pyrite veinlets.
35.0 – 36.3	Disseminated pyrite and rare chalcopyrite.
36.6	Quartz-chalcopyrite-pyrite-molybdenite veinlet.
36.7	Quartz-scheelite veinlet.

37.5	Quartz-pyrite vein.
37.6 – 37.8	Disseminated pyrite.
38.4 – 39.0	Quartz-chalcopyrite-pyrite veinlets.
39.3	Quartz-chalcopyrite veinlet.
39.6	Quartz-chalcopyrite veinlet.
39.9	Quartz-chalcopyrite-pyrite veinlet.
40.2	Chalcopyrite and molybdenite, without associated veinlet.
40.5	Quartz-chalcopyrite-pyrite veinlets.
40.8	Quartz-chalcopyrite-molybdenite veinlets.
41.1	Quartz-pyrite-chalcopyrite-molybdenite veinlets.
41.5	A little disseminated pyrite.
42.1	A little disseminated pyrite.
43.3	Quartz-chalcopyrite veinlet.
43.4	A little disseminated pyrite.
43.9 – 44.2	Two pyrite veinlets.
44.3	Quartz-molybdenite veinlet.
44.5 – 45.4	Quartz-pyrite veinlets and disseminated pyrite.
45.5	Quartz-chalcopyrite and quartz-pyrite veinlets.
46.0	Quartz-molybdenite-pyrite and quartz-pyrite veinlets.
46.3	Disseminated pyrite.
46.6	Isolated molybdenite.
47.2	Disseminated pyrite.
48.5 – 51.5	Disseminated pyrite, rare chalcopyrite and trace molybdenite.
50.0	Quartz-pyrite-chalcopyrite veinlet.
52.0	Disseminated chalcopyrite and ?bornite.
52.3	Quartz-chalcopyrite veinlet.
52.7	Quartz-pyrite veinlet.
54.6 – 56.4	Sparse disseminated chalcopyrite.
57.3	Pyrite-molybdenite veinlet.
57.6	Pyrite veinlet.
57.6 – 63.7	Sparse disseminated pyrite and chalcopyrite.
60.0	Quartz-chalcopyrite vein and pyrite veinlet.
65.2 – 66.8	Disseminated pyrite.
66.1 – 68.3	Fractured, with loss of 0.5 m core
66.8 – 67.1	Aplite.
67.7	Disseminated pyrite.
68.9	Pyrite and chalcopyrite, disseminated and in veinlet.
70.7 – 71.9	Much irregular fracturing and veining, some with calcite.
72.5 – 72.8	Much irregular fracturing and veining, some with calcite.
75.6	Pyrite and molybdenite, associated with irregular fracturing.
76.2	Alkali feldspar is whitened (kaolinised). Plagioclase altered to white mica and also to ? analcime.
78.0	Chalcopyrite veinlet.
79.1	Quartz-pyrite veinlet, and disseminated pyrite.
80.2	Isolated molybdenite.
80.8	Two quartz-pyrite veinlets, with trace chalcopyrite.
81.1	Disseminated pyrite and chalcopyrite.
81.4 – 82.0	Disseminated pyrite and chalcopyrite, continuing, less abundant, to 82.6.
81.8	Black chloritic fracture coating.
82.6	Isolated molybdenite.
83.7	Disseminated pyrite.
84.4	Quartz-chalcopyrite-pyrite veinlet.
84.7	Patch of pyrite.
85.0	Patch of pyrite.
86.4	Patches of pyrite, with some associated quartz.
87.8	Isolated molybdenite.
88.1	Disseminated pyrite.
88.4	Disseminated pyrite, chalcopyrite and molybdenite.
89.0	Pyrite veinlet. Continuing disseminated pyrite.
90.2	Quartz-pyrite veinlet.
90.8	Disseminated pyrite and chalcopyrite.
92.0	Disseminated pyrite.
92.7	Pyrite veinlet.
93.3	Disseminated pyrite.
93.6	Pyrite veinlet.
95.1	Quartz-molybdenite veinlet and pyrite veinlet.
98.1	Disseminated chalcopyrite.
99.7	Patch of chalcopyrite
100.6	Disseminated chalcopyrite and isolated molybdenite.
100.9	Irregular quartz and chalcopyrite.
102.4	Disseminated pyrite and isolated molybdenite.
102.9 – 103.6	Disseminated pyrite and chalopyrite.
103.8 – 103.9	Disseminated pyrite and pyrite veinlet.
105.2	Pyrite veinlet and associated dissemination.
107.6	Veinlet trending 30° to length of core, with associated pyrite and molybdenite.
108.2	Pyrite-chalcopyrite veinlet and associated dissemination.
108.8	Disseminated chalcopyrite and pyrite.
112.1	Disseminated pyrite, chalcopyrite and possibly bornite.
c.110.0	Broken, with 1 m of core loss.
112.2 – 113.4	Altered microdiorite dyke, composed of plagioclase with abundant calcite and sericite, a little chlorite and quartz, accessory ilmenite and trace disseminated chalcopyrite.
113.7	Disseminated pyrite.
114.6	Pyrite veinlet and dissemination.
116.7	Disseminated pyrite.
c.117.0	Broken, with some core loss.
119.5	Disseminated molybdenite.
119.9	Disseminated pyrite.
121.0 – 121.3	Disseminated pyrite.
121.6	Isolated molybdenite.

121.9	Disseminated pyrite, chalcopyrite, arsenopyrite and molybdenite, sporadic molybdenite continuing to 123.1.
124.4	Quartz-pyrite veinlet and disseminated pyrite.
125.9	Disseminated chalcopyrite.
126.2	Isolated molybdenite.
126.6	Disseminated chalcopyrite and molybdenite.
127.4	Isolated molybdenite.
127.8	Isolated molybdenite.
128.0 – 128.3	Disseminated molybdenite and chalcopyrite. Chalcopyrite continues sporadically to 131.0.
132.0	Isolated molybdenite.
132.6	Isolated molybdenite.
133.5	Two pyrite veinlets.
134.3	Isolated molybdenite.
134.7	Isolated chalcopyrite.
135.3	Pyrite veinlet and dissemination.
135.8	Isolated molybdenite.
136.2	Disseminated pyrite.
136.9	Disseminated pyrite.
137.8	Isolated molybdenite.
138.2	Isolated molybdenite.
138.4	Calcite veins.
138.7	Disseminated pyrite.
140.4	Calcite veins.
140.7	Disseminated pyrite.
141.1	Clusters of pyrite crystals.
141.4	Disseminated pyrite, chalcopyrite and molybdenite.
142.0	Pyrite disseminated and in longitudinal veinlets.
142.6	Disseminated chalcopyrite.
143.3	Disseminated chalcopyrite and possibly bornite.
144.2	Fracture coated with molybdenite.
144.3	Calcite vein.
144.5 – 144.8	Narrow quartz veinlets and disseminated pyrite and chalcopyrite.
144.5	Fracture coated with molybdenite.
145.1 – 145.8	Fractures coated with molybdenite, and some disseminated molybdenite and chalcopyrite.
146.9	Disseminated chalcopyrite.
147.2	Disseminated chalcopyrite and molybdenite.
147.8	Disseminated chalcopyrite.
148.1	Disseminated chalcopyrite and molybdenite.
149.4	Isolated molybdenite and trace disseminated pyrite and chalcopyrite.
149.7 – 151.8	Disseminated pyrite, chalcopyrite and molybdenite.
152.4 – 160.0	Disseminated pyrite, chalcopyrite, very rare molybdenite, and possibly bornite.
155.4	Fracture coated with pyrite and molybdenite.
155.6	Calcite veining. Pyrite and molybdenite on fracture surface, with associated pyrite dissemination.
157.3	Calcite veining.
159.4	Molybdenite on fracture surface.
161.2	A little disseminated chalcopyrite and molybdenite.
161.5	Disseminated chalcopyrite.
162.0	Bornite with quartz.
162.8	Chalcopyrite and bornite.
163.4	Molybdenite on fracture surface.
163.7	Cluster of chalcopyrite grains. Trace molybdenite, continuing to 164.3
164.9	Isolated molybdenite.
165.2	Isolated molybdenite. Calcite vein.
165.5	Chalcopyrite.
165.8	Isolated molybdenite.
166.7	Disseminated chalcopyrite and molybdenite.
170.1	Molybdenite fracture-coating. Pyrite in and near veinlet.
170.4	Cluster of pyrite. Isolated molybdenite.
171.6	Chalcopyrite.
172.5	Isolated molybdenite.
173.9 – 174.3	Disseminated chalcopyrite and bornite.
175.0	Cluster of chalcopyrite.